Combined water table and temperature dynamics control CO₂ emission estimates from drained peatlands under rewetting and climate change scenarios

Tanja Denager[1], Jesper Riis Christiansen[2], Raphael Johannes Maria Schneider[1], Peter Langen[3], Thea Quistgaard[3], Simon Stisen[1]

[1] Department of Hydrology, Geological Survey of Denmark and Greenland, Copenhagen, Denmark
[2] Forest and Landscape Ecology, Department of Geoscience and Nature Management, Copenhagen University, Denmark
[3] Department of Environmental Science, Atmospheric Emissions & Modelling, Aarhus University, Roskilde, Denmark

Correspondence to: Tanja Denager (tad@geus.dk)

Abstract:

This study integrates process-based hydrological modeling and empirical CO_2 flux modeling at a daily temporal resolution to evaluate how peatland hydrology influence CO_2 emissions under scenarios of rewetting and climate change.

Following the calibration of a three-dimensional transient groundwater flow model for a peat-dominated catchment, daily groundwater table dynamics were simulated to represent hydrological conditions in drained peat soils. These simulations were coupled with an empirical CO_2 flux model, developed from a comprehensive daily dataset of groundwater table depth, temperature, and soil CO_2 flux measurements. The empirical CO_2 flux model captures a clear temperature-dependent response of soil CO_2 emissions to variations in groundwater table depth.

By applying this coupled modeling framework, we quantified CO_2 emissions at daily timescales. The results demonstrate that incorporating both temperature sensitivity and high-resolution temporal variability in water level significantly influences projections of CO_2 fluxes. Especially the co-occurrence of elevated air temperature and low groundwater table significantly influence CO_2 emissions under scenarios of rewetting and climate change. These insights highlight the importance of including changing climate conditions in future peatland management strategies for emission inventories.

The study illustrates the value of combining detailed hydrological simulations with emission models. It also emphasizes the need for detailed monitoring of greenhouse gas emissions across multiple sites and the development of robust empirical models that can be generalized and spatially upscaled.

Introduction

Drained peatlands are widely accepted as being net greenhouse gas (GHG) sources and rewetting of peatlands is considered an effective means of overall net GHG emission reduction (Leifeld et al., 2019). The depth of the groundwater table below the surface i.e. the water table depth (WTD) largely controls the annual emissions of carbon dioxide (CO_2) and methane (CH_4) from organic soils, where deeper WTD results in CO_2 emissions and a shallow WTD increases CH_4 emissions (Evans et al., 2021). Despite triggering CH_4 emissions, rewetting of organic soils will still lead to a net long-term reduction of GHG emissions (Günther et al., 2020). However, current estimates of GHG emissions from drained and rewetted peatlands are still quite uncertain due to a lack of long-term monitoring and simplified modeling approaches.

Commonly adopted methodologies for estimating contribution of organic soils in national GHG inventories (Arents et al., 2018; Evans et al., 2021; Koch et al., 2023; Tiemeyer et al., 2020) are based on empirical response functions between long-term annual mean WTD estimates from data-driven machine learning (ML) models (Bechtold et al., 2014; Koch et al., 2023) and observed net ecosystem GHG budgets (Tiemeyer et al. 2020). Those methodologies allow regional upscaling and integration into national emission estimates.

However, significant variability in the observed net ecosystem carbon balance (NECB) used to derive the empirical relationship can be attributed to site-specific factors, including intra-annual (seasonal) WTD and temperature dynamics (Tiemeyer et al., 2020) caused by fluctuating climate. The current GHG inventory methods are not suited to account for extremes such as drought and flooding that have a profound, but temporally limited (days, weeks or months) impact on WTD. Especially the frequency and severity of droughts can have major impacts on the CO_2 emissions as WTD increases together with temperature (Olefeldt et al., 2017). Therefore, temperature changes also directly impact GHG emissions, as soil CO_2 and CH_4 production are temperature sensitive. Currently, the impact of short-term compound events (e.g., simultaneous warm and dry conditions (Zscheischler et al., 2020) on annual CO_2 emissions from peat soil is little known. Such events can lead to consequences like a deep groundwater table, highlighting the need for improved understanding of how climate variability and long-term change (Olefeldt et al., 2017) affect future CO_2 emissions from both drained and rewetted peatlands.

For Denmark, it is generally expected that, as a result of climatic changes, annual mean WTD will decrease (water tables closer to surface). However, this decrease in annual mean WTD is primarily attributed to an decrease in WTD during the wetter winter months, while warmer future summers are anticipated to experience minimal decrease or even increase in summer WTD (water tables deeper below the surface) and more prolonged periods with increased WTD (Henriksen et al., 2023; Seidenfaden et al., 2022).

The ML and statistical models of annual mean WTD (Bechtold et al., 2014; Koch et al., 2023) utilized in current national GHG inventories (Gyldenkærne et al., 2025; Koch et al., 2023; Nielsen et al., 2025b; Tiemeyer et al., 2020) effectively reflect the spatial variability at the national scale, but most current ML WTD models are temporally invariant and account for neither inter-annual (between-year) variability nor seasonal or intra-annual variability in WTD or temperature. . To establish WTD-CO_2 relations at intra-annual time scales, capable of capturing the impact of short-lived extreme events such as droughts and inundations, WTD time series at these finer temporal resolutions are required. For this, process-based transient 3D hydrological models capable of integrating unsaturated-saturated flow models to predict spatial and temporal variability of WTD are highly useful. Combined with the WTD-CO_2 relation we claim these model outputs can be used to calculate the CO_2 emissions on daily, seasonal, and inter-annual timescales.

79 Such hydrological models provide the potential for improving our estimation of peatland hydrology
80 and thereby the spatio-temporal WTD variability. Improved representation of temporal variability of
81 WTD are needed for refining the current and future GHG estimates that cannot be derived using the
82 simple application of IPCC default emission factors (IPCC, 2014). Process-based hydrological models
83 offer the opportunity to assess the effect of different management strategies and environmental
84 conditions, such as rewetting and climate change.

85 Process-based hydrological models are increasingly being applied to study dynamics of peatland
86 hydrology (Mozafari et al., 2023). For instance, Land Surface Models (LSM) (Bechtold et al., 2019;
87 Largeron et al., 2018; Shi et al., 2015; Yuan et al., 2021) are employed to analyze the soil–plant–
88 atmosphere exchange processes of water, energy and carbon. However, most LSM's rely on a
89 simplified conceptual representation of hydrologic processes and are characterized by coarse spatial
90 scales.

91 Of the studies applying fully integrated unsaturated-saturated flow models for peatland hydrology,
92 some focus on site or field--scale models (Friedrich et al., 2023; Haahti et al., 2015; Java et al., 2021;
93 Stenberg et al., 2018) while others apply the models at catchment scale (Ala-aho et al., 2017; Duranel
94 et al., 2021; Friedrich et al., 2023; Jutebring et al., 2018; Lewis et al., 2013). A catchment scale
95 approach with water balance closure is particularly important for climate change impact predictions,
96 since the boundary conditions to the peatlands will also be affected by climate change. Similarly, the
97 use of catchment scale models is important because impact evaluations of peatland management
98 scenarios, such as rewetting, can also include impacts on streamflow and groundwater levels in
99 neighboring areas.

100 The objectives of this study were to 1) estimate current and predict the future hydrology and soil CO_2
101 emissions in a Northern European drained peatland and 2) investigate the role of rewetting and
102 climatic extremes on annual CO_2 emissions. To achieve these objectives, we used a transient
103 physically-based hydrological 3D model to predict daily WTD for a case study area, the Tuse Stream
104 catchment, representing a typical degraded Danish peatland. Secondly, we developed an empirical soil
105 CO_2 flux (fCO_2) model based on coupled CO_2 flux, WTD and temperature observations for a similar
106 Danish peatland (Nielsen et al., 2025a), capable of making daily predictions. Combining the
107 mechanistic hydrological model and the empirical emission model enabled the estimation of daily soil
108 CO_2 fluxes under current conditions as well as scenarios of rewetting and future climate, while
109 accounting for the impact of climatic variability and extremes.

Data and methodology

Study area

111
112 Tuse Stream catchment is located on the island of Zealand in the eastern part of Denmark (Figure 1a).
113 The total area encompasses 107 km^2 of which 19 km^2 are peat soil. The areal extent of peat soil was
114 determined using a national map of organic soils (Adhikari et al., 2014). The largest continuous peat
115 area within the catchment is a 13 km^2 drained fen located in a river valley (Figure 1c) in the low-lying
116 part of the catchment. The peat soil area is primarily used for agriculture. In small parts of the area,
117 the drainage has been stopped to restore the natural hydrologic regime. The measured peat layer
118 thickness extends from 0.4 to 3.5 meters, below which alluvial sand deposits are typically found.
119 Generally, the deeper geology in the area can be characterized as clay-dominated glacial till deposits.
120 The catchment is characterized by flat topography, with the southern part of the catchment being
121 hillier. The climate conditions are humid and temperate. The catchment receives about 737 mm of
122 precipitation per year (1990-2024) and has an annual mean temperature of 9°C (Scharling, 1999a, b).
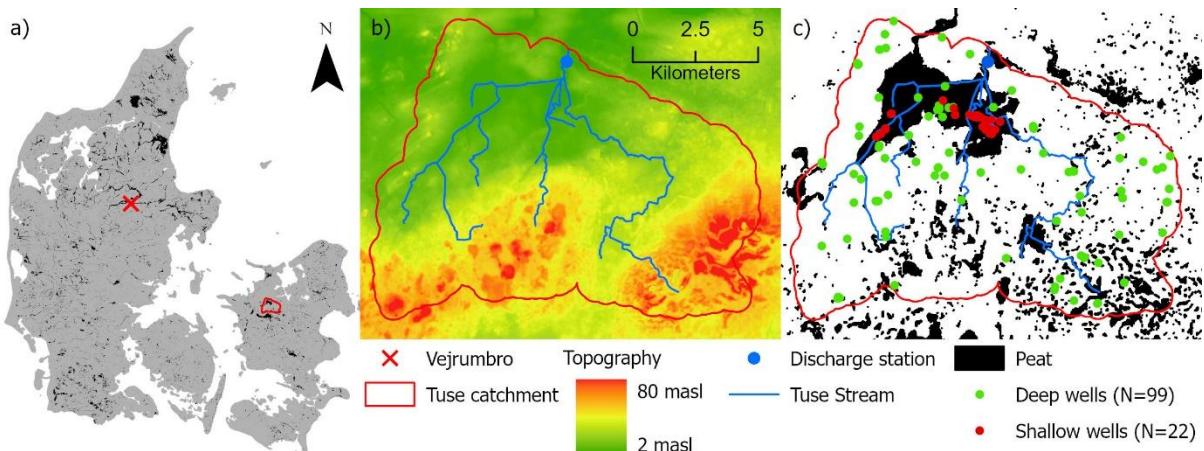
123

124 *Figure 1: a) Location of Tuse Stream catchment and the Vejrumbro site, b) topography and stream network of Tuse Stream*
125 *catchment, masl: meter above sea level, c) location of organic soil and observation wells in the Tuse Stream catchment.*

126 Shallow WTD in the drained organic soils is monitored in 22 groundwater wells (2-3.5 meters deep)
127 (Figure 1c). The wells are fully screened and WTD is automatically logged with pressure transducers at
128 an hourly basis (aggregated to daily values) and verified with manual measurements. All WTD data are
129 available in the Danish National Well Database (Jupiter, 2025). In this study, we define the water table
130 depth (WTD) as positive when located below the surface and negative when above the surface.
131 Monitoring data includes additional point measurements and timeseries of groundwater head from 99
132 deep wells installed in mineral soils throughout the catchment (Figure 1c). In the model setup, water
133 extraction in 40 abstraction wells is included based on data from the Danish National Well Database in
134 May 2020 (Henriksen et al., 2020) and implemented as yearly mean abstraction evenly distributed on
135 the daily model timesteps. Daily discharge is monitored at the catchment outlet at Tuse Stream (Figure
136 1b).

137 ## Hydrological modelling
138 The focus of the hydrological modelling in this study is to adequately simulate shallow groundwater
139 levels and their dynamics for the peatland area in the Tuse Stream catchment. The fen peatland in
140 Tuse Stream catchment is largely fed by groundwater discharge from the upstream catchment,
141 emphasizing the need to develop a coupled groundwater surface water model at catchment scale. In
142 addition, the objective of utilizing the model for climate change impact assessments requires a
143 catchment scale approach with a deep groundwater component to represent changes in groundwater
144 and surface water discharge to the peatland as well as changes in the boundary conditions. The
145 catchment scale approach also facilitates the combined calibration and evaluation of the total water
146 balance and peatland WTD by constraining the model with observed streamflow at the outlet as well
147 as peatland groundwater level dynamics.

148 The model is set up as a transient, distributed, coupled surface-groundwater model and executed
149 within the hydrological modeling framework MIKE SHE (DHI, 2022; Graham and Butts, 2005). MIKE SHE
150 combines full 3D groundwater flow coupled with a gravity flow module in the unsaturated zone, 2D
151 overland flow and 1D river flow routing in streams (DHI, 2019) (Figure S1). The simplified gravity flow
152 module for unsaturated flow assumes a uniform vertical gradient and ignores capillary forces but
153 provides a suitable solution for the time varying recharge to the groundwater table based on
154 precipitation and evapotranspiration (DHI, 2022).

155 The model is a modified sub-model of the National Hydrological Model of Denmark (DK-model),
156 developed at the Geological Survey of Denmark and Greenland (GEUS) (Henriksen et al., 2020; Stisen
157 et al., 2019). The geological model is interpreted in a horizontal 100 meter grid. The numerical model is

158 calibrated in the same 100 meter resolution, with the saturated zone consisting of 11 computational
159 layers of varying thickness. The top model layer has a uniform thickness of 2 meters, which is also
160 applied to the peat layer areas. The bottom level of the groundwater model is defined by the
161 prequaternary chalk that underlies the Island of Zealand, which in the Tuse Stream catchment is
162 located in a depth of approximately 150-250 meters below surface.

163 The time-varying constant head boundary conditions at the sub-model boundary are defined from the
164 operational National Hydrological Model setup (Henriksen et al., 2020). The observed forcing data of
165 precipitation, temperature and reference evapotranspiration are provided by the Danish
166 Meteorological Institute (DMI) as gridded daily data in 10 km resolution for precipitation and 20 km
167 resolution for evapotranspiration and temperature (Scharling, 1999a, b; Stisen et al., 2011). The model
168 employs a maximum timestep of one day, at which the meteorological variables are fed into the
169 model. The model was provided with a hotstart file from an initial model run.

170 Spatial and temporal distributions of root depth and LAI are based on classes (Figure S2 and Table S1)
171 where the peat, forest, agricultural and open nature land use classes have yearly cycles of LAI and root
172 depth (Figure S3). Likewise, soil type is spatially distributed (Figure S2) and based on the three classes
173 peat, sand and clay (Table S2). In the vertical direction, the soil columns in the unsaturated zone
174 module are divided into 40 cells from top to bottom; 30x0.1m, 5x1m and 5x5m. Technically, the
175 unsaturated zone is parameterized to 33 m depth, but during simulation limited to the top of the
176 simulated groundwater table. We implemented uniform vertical water retention characteristics of
177 peat, while clay and sand water retention characteristics were defined separately for the depths 0-30
178 cm (horizon A), 30-70 cm (horizon B) and >70 cm (horizon C). Soil parameterization is freely adapted
179 from (Børgesen et al., 2009) and detailed in Table S3.

180 MIKE SHE allows incorporation of drainage systems, representing both artificial and natural drains. The
181 drainage system bypasses the slow water movement in aquifers by providing a short-cut from e.g. the
182 agricultural field to the nearest stream. The amount of water routed by drains from the saturated zone
183 to local surface water bodies is calculated using a linear reservoir model, where the difference
184 between groundwater head and drain level is multiplied by a drain time constant (dt). The drain level is
185 defined by a drain depth (dd) set relative to surface level. Hence, drainage in any given model cell only
186 occurs if the simulated groundwater level exceeds the drainage level (DHI, 2022). The drain time
187 constant and drainage depth in each model grid cell are distributed across the model domain
188 according to the five land use classes (Figure S2 and Table S1).

189 The model parameter sensitivity analysis and subsequent calibration prioritized parameters affecting
190 the shallow WTD in the peat soil and the overall water balance in the catchment. A list of model
191 parameters can be seen in Table S3. Parameter values not included in the calibration process are
192 obtained from the National Hydrological Model parametrization.

Calibration method

194 We used the Pareto Archived Dynamically Dimensioned Search (PADDS) algorithm (Asadzadeh and
195 Tolson, 2013) available within the optimization toolkit Ostrich (Matott, 2019). PADDS is a multi-
196 objective optimizer and obtains the pareto front across multiple objective function groups, enabling
197 post-weighting of individual objective functions. Throughout the calibration routine, Ostrich minimized
198 the weighted sum of squared error (WSSE) of each of the objective function groups. The PADDS
199 algorithm was run with the user settings of maximum 1000 iterations. The period 2010-2013 was used
200 as a calibration spin-up period and the model performance was evaluated for the 2014-2023
201 calibration period.

202 Calibration was performed against three objective function groups: $KGE_{WTD\_modified}$, $r_{spatial}$ and
203 $KGE_qME_{head}ME_{amp}$. The $KGE_{WTD\_modified}$ objective group is used to optimize the model performance with
204 respect to the WTD in peatlands. KGE is the Kling-Gupta Efficiency and consists of three terms: the
205 Pearson correlation coefficient r, a term representing the measure of variability α and a bias term β. In
206 KGE, β is a unitless measure of the bias specified as the ratio between the sum of simulated and
207 observed values (β = ∑sim/∑obs). As we use KGE to optimize the WTD (and not hydraulic head), the
208 operational sign can be both negative (water table above surface/inundation) and positive (water
209 table below surface), violating the idea of optimizing β as the ratio of sums of values with possibly
210 alternating operational signs. Therefore, we are using $KGE_{WTD\_modified}$ where β is replaced by the mean
211 error (ME) (Table 1). This modification requires that the order of magnitude of the ME_{WTD} is
212 comparable to the errors on the other terms in KGE. In our case this is ensured by the fact that the
213 mean observed WTD values range between approximately 0.3-0.6 m, resulting in ME_{WTD} values
214 typically below 0.5 m. Alternatively, the ME_{WTD} term could be scaled within the KGE_{WTD} equation.

215 The calibration using the $KGE_{WTD\_modified}$ as objective function group aims at achieving the best overall
216 agreement between simulated and observed WTD. However, during first calibration experiments, we
217 found that this objective function group primarily focuses on the temporal dynamics of WTD. To
218 improve the representation of the spatial variability of the mean WTD, the correlation coefficient
219 ($r_{spatial}$) was included as an additional objective function group (Table 1).

220 $KGE_qME_{head}ME_{amp}$ is an objective function group that combines three performance criteria: the Kling-
221 Gupta Efficiency performance criterion for discharge (KGE_q), the mean error of hydraulic head in
222 deeper aquifers (ME_{head}) and the mean error of annual amplitude of hydraulic head in the deeper
223 aquifers (ME_{amp}). For a detailed description of the implementation of ME_{amp} as objective function see
224 (Henriksen et al., 2020). This objective function group was included to optimize the overall water
225 balance and streamflow dynamics expressed through the discharge at the catchment outlet (KGE_q), to
226 match the general water level in the deeper aquifers across the catchment (ME_{head}), and to match the
227 natural seasonal variations in hydraulic head (ME_{amp}). As the metrics of KGE_q, ME_{head} and ME_{amp} are
228 combined into one objective function group, we need to weigh the observations, to ensure that KGE_q,
229 ME_{head} and ME_{amp} affect the objective group of $KGE_qME_{head}ME_{amp}$ approximately equally. This was done
230 based on WSSE from a model run with initial parameter values.

231 *Table 1: Objective functions metrics. KGE stands for Kling-Gupta Efficiency.*

Objective function group	Observations	No. of observation wells	Metric	Abbreviation	Equation	Range	Optimum value
$KGE_{WTD\_modified}$	Daily WTD in shallow wells (in peat)	22	Modified KGE on WTD	$KGE_{WTD\_modified}$	$1 - \sqrt{(r_{WTD}-1)^2 + (\alpha_{WTD}-1)^2 + (ME_{WTD})^2}$ Where, $ME_{WTD} = \frac{1}{n}\sum_{i=1}^{n} WTD_{sim_i} - WTD_{obs_i}$	[-∞;1]	1
$r_{spatial}$	Mean WTD over the calibration period	22	Spatial correlation of the mean WTD	$r_{spatial}$	$r(\overline{WTD_{sim}}, \overline{WTD_{obs}})$	[-1;1]	1
$KGE_qME_{head}ME_{amp}$	Discharge	1	KGE on discharge	KGE_q	$1 - \sqrt{(r_q-1)^2 + (\alpha_q-1)^2 + (\beta_q-1)^2}$	[-∞;1]	1
	Hydraulic head in deep wells (in mineral soil)	66	Mean error on hydraulic heads	ME_{head}	$\frac{1}{n}\sum_{i=1}^{n} head_{sim_i} - head_{obs_i}$	[-∞;∞]	0

| | | 8 | Mean error on yearly amplitude of hydraulic heads | ME_{amp} | $\frac{1}{n}\sum_{i=1}^{n} A_{sim_i} - A_{obs_i}$ | $[-\infty;\infty]$ | 0 |

232 WTD: water table depth [m], q: discharge [m/s], head: hydraulic head [m], A: amplitude [m]

233 A local sensitivity analysis based on initial parameter values from Table S4 was performed and values
234 of composite scaled sensitivity (CSS) were obtained. Selection of free calibration parameters were
235 based on the criterion that parameters were included if their CSS was larger than 0.05*CSS of the
236 parameter with the highest CSS. The resulting 11 free parameters are indicated with grey in Table S4.
237 Other parameters were kept at the values listed in Table S4 or tied to the calibration parameters.

Hydrological simulations of historical and future climate

239 The calibrated hydrological model was run for the historical simulation period of 1990-2023 using
240 observed climate forcing data (Scharling, 1999a, b; Stisen et al., 2011). Future hydrological projections
241 are derived from simulations using the hydrological model forced by climate model projections,
242 including precipitation, air temperature (T_{air}), and potential evapotranspiration. The resulting impacts
243 on groundwater levels, as simulated by the hydrological model, are evaluated. We used 17 climate
244 models (Table S5) with the Representative Concentration Pathway 8.5 (RCP8.5), which represents the
245 RCP scenario (2.6-8.5) leading to the highest emissions and strongest impact of climate change. The
246 climate model outputs are generated and bias corrected by Pasten-Zapata et al. (2019), and the Global
247 and Regional Circulation (GCM, RCM) models originate from the Euro-CORDEX project (Jacob et al.,
248 2014).

249 The climate simulations cover three 30-year periods: the reference period (1991-2020), the mid-
250 century (2041-2070) and the end-century (2071-2100). All 51 climate simulations (17 climate models ×
251 3 periods) were first run using the initial potential head from the national model climate simulations
252 (Henriksen et al., 2020). Subsequently, they were rerun using the mean potential head for the
253 respective 30-year period as the initial potential head.

Empirical CO_2 emission models

Implementation of annual CO_2 emission model

256 Recent studies established a functional relationship between the annual net ecosystem carbon balance
257 (NECB) for CO_2 and the mean annual WTD (Koch et al., 2023; Tiemeyer et al., 2020) by fitting a
258 nonlinear Gompertz function. Like in Koch et al. (2023) and Tiemeyer et al. (2020), this study considers
259 NECB as only CO_2 fluxes, excluding methane (CH_4) and other carbon exports such as dissolved or
260 particulate organic carbon. We apply the WTD functional relationship for CO_2 from Koch et al. (2023),
261 which is fitted to Danish flux data, and refer to it as the *Annual WTD model*. The *Annual WTD model*
262 demonstrates a systematic relationship in which CO_2 flux from NECB increases with annual WTD in the
263 interval between 7 cm and 50 cm, above which an asymptotic level of 10 Mg CO_2-C ha^{-1} yr^{-1} is reached
264 (Koch et al., 2023). The *Annual WTD model* is therefore not sensitive to changes in WTD deeper than
265 approximately 50 cm. At WTD levels less than 7 cm, the *Annual WTD model* suggests CO_2 uptake;
266 however, this element is not included in our analysis which only models CO_2 emission.

Derivation and implementation of daily CO_2 emission model

268 For our empirical model to predict daily soil CO_2 fluxes (fCO_2) we assume that the WTD dependent
269 NECB (Tiemeyer et al. 2020, Koch et al. 2023) is driven mainly by the response of soil respiration to
270 WTD and T_{air}, as gross primary photosynthesis (GPP) and aboveground autotrophic respiration is
271 mostly dependent on light availability and plant phenology (Rodriguez et al., 2024). This allows scaling
272 to match the NECB magnitude but maintains integrity in the regulation of WTD on soil CO_2 fluxes.

273   Using a unique and comprehensive coupled dataset (Nielsen et al., 2025a) of daily mean net soil CO_2

274   fluxes, T_{air} and WTD for six spatial replicate measurement points, we develop a coupled temperature

275   and WTD dependent empirical soil CO_2 flux model, hereafter referred to as the *Daily WTD-T_{air} model*.

276   The model essentially scales the WTD-fCO_2 relation to T_{air}. The dataset Nielsen et al. (2025a) is from a

277   drained fen, called Vejrumbro (Figure 1), with similar characteristics (soil type, climate, land use

278   history) as the peat area in the Tuse Stream catchment (see methodological details in Nielsen et al.

279   (2025a). The soil net CO_2 fluxes, WTD and T_{air} were measured automatically for one year (2022-2023)

280   (Nielsen et al., 2025a) and we used a subset of fluxes measured for six spatial replicates 5-6 times per

281   day, resulting in a dataset of 10950 – 13140 individual fluxes covering 365 days (Nielsen et al., 2025a).

282   Implementation of CO_2 flux models

283   Spatially distributed net soil CO_2 fluxes are calculated at a 100-meter scale across the 13 km²

284   contiguous peatland area (Figure 1) with the *Annual WTD model* and the *Daily WTD-T_{air} model*,

285   respectively, using WTD at a 100-meter scale (hectare scale) and a uniform T_{air}. Afterwards the

286   spatially distributed soil CO_2 fluxes are aggregated to represent the spatial mean of the 13 km²

287   peatland area.

288   First, we applied the *Annual WTD model* and the *Daily WTD-T_{air} model* for the historical simulation

289   period of 1990-2023, using spatiotemporal distributed WTD from the calibrated hydrological model.

290   Afterwards, the empirical CO_2 models are utilized on each of the 17 climate projections for T_{air} and

291   WTD. Daily T_{air} for the Tuse Stream catchment peatland area is taken directly from the 17 bias

292   corrected climate projections, while daily spatial WTD is a model output from the 17 hydrological

293   simulations, when running the hydrological model with the forcing data (precipitation, temperature

294   and evapotranspiration) from the 17 climate projections. Thereby, we are able to quantify the

295   variability in soil CO_2 flux among the 17 climate projections for each of the simulation periods and

296   among the 30 years within each of the simulation periods.

297   Design and application of rewetting scenarios

298   For impact evaluations of peatland management scenarios, such as rewetting, on the annual CO_2

299   emissions, we define three rewetting scenarios: A, B and C. These scenarios are implemented through

300   controlled modifications of the simulated WTD in peatland grid cells. This method of representing

301   rewetting scenarios does not involve structural modifications to the hydrological model and assumes

302   changes in WTD without accounting for process-based feedback mechanisms within the coupled

303   surface–subsurface hydrological system. Therefore, the rewetting scenarios cannot be interpreted as

304   real-life management practices. All rewetting scenarios were applied for 1990 to 2023, representing

305   the climatology for this period and generating 34-year time series of rewetted WTD.

306   The scenarios are meant to illustrate different rewetting impacts on WTD, representing wetter winters

307   (A), uniform shift in WTD (B) and wetter summers (C), but all with the same long-term mean WTD. In

308   Scenario A, the daily groundwater table is elevated when it is above the long-term (34-year) mean

309   water table resulting in unchanged water table levels during summer but an increase in winter.

310   Scenario B uniformly raises the water table by a constant scalar, while Scenario C applies the same

311   scalar increase to water table while simultaneously reducing the annual amplitude by half. The

312   modifications of the simulated WTD are implemented using the following equations:

313
$$WTD_{i_{rewet\,A}} = \begin{cases} WTD_i, & if\ WTD_i \geq \overline{WTD} \\ WTD_i + 2.5 \cdot (\overline{WTD} - WTD_i), & if\ WTD_i < \overline{WTD} \end{cases} \qquad [2]$$

314

315
$$WTD_{i_{rewet\,B}} = WTD_i - (\overline{WTD} - \overline{WTD_{rewet\,A}}) \qquad [3]$$

316

317 $$WTD_{i_{rewet\ C}} = \overline{WTD_{rewet\ B}} + 0.5 \cdot (WTD_{i_{rewet\ B}} - \overline{WTD_{rewet\ B}}) \hspace{2cm} [4]$$

318

319 where $WTD_{i_{rewet\ A}}$, $WTD_{i_{rewet\ B}}$ and $WTD_{i_{rewet\ C}}$ is the daily WTD in a grid cell for rewetting

320 scenario A, B and C, respectively. WTD_i is the daily WTD in a grid cell from the calibrated hydrological

321 model. $\overline{WTD}$ is the long-term (34-year) mean WTD in a grid cell from the historical period of the

322 calibrated hydrological model. $\overline{WTD_{rewet\ A}}$ and $\overline{WTD_{rewet\ B}}$ are long-term (34-year) mean WTD in a

323 grid cell from the rewetting scenario A and B, respectively.

324 Bootstrapping means of future climate CO_2 emissions

325 We applied a bootstrap resampling approach to estimate the uncertainty in the mean values of soil

326 CO_2 flux. Specifically, we resampled the means over the 17 climate models, each containing 30 annual

327 values, with replacement. This process was repeated 10,000 times to construct bias-corrected and

328 percentile-based 95% confidence intervals around the bootstrapped means.

329

Results

Hydrological model

Calibration of the hydrological model

The model calibration, running 1000 model evaluations based on three objective function groups, using Ostrich ParaPADDS optimizer with 40 parallel model executions, took ~24 hours on a Xeon Et-4850 @2,20 GHz Server. The calibration resulted in 203 non-dominated solutions forming a three-dimensional pareto front. Figure 2 presents scatterplots of the three objective functions, illustrating the trade-offs between them. Especially, there is a clear trade-off between the two objective functions addressing temporal dynamics (KGE_{WTD}) and spatial dynamics ($r_{spatial}$), as illustrated in Figure 2a.

The number of non-dominated solutions and the trade-offs illustrate that several parameter sets can be considered and that an ensemble of parameter sets could be selected. For the purpose of further analysis and climate change impact assessments, however, we select one balanced solution from the non-dominated solutions, through a stepwise procedure. First, a pre-screening was performed with performance criteria for WTD of KGE_{WTD} larger than 0.6, for discharge of $KGE_{discharge}$ larger than 0.6 and for hydraulic head in deeper wells of ±1 m, for ME_{head} and ME_{amp}, respectively. Afterwards, the balanced parameter set was selected as the solution with the highest spatial correlation ($r_{spatial}$).

The selection procedure was designed to prioritize accurate simulation of the temporal dynamics of peatland WTD, while maintaining strong performance across additional objective functions and maximizing spatial correlation accuracy. Initial calibration efforts indicated that achieving a KGE_{WTD} value greater than 0.6 was necessary to ensure an adequate alignment between the simulated and observed WTD time series.
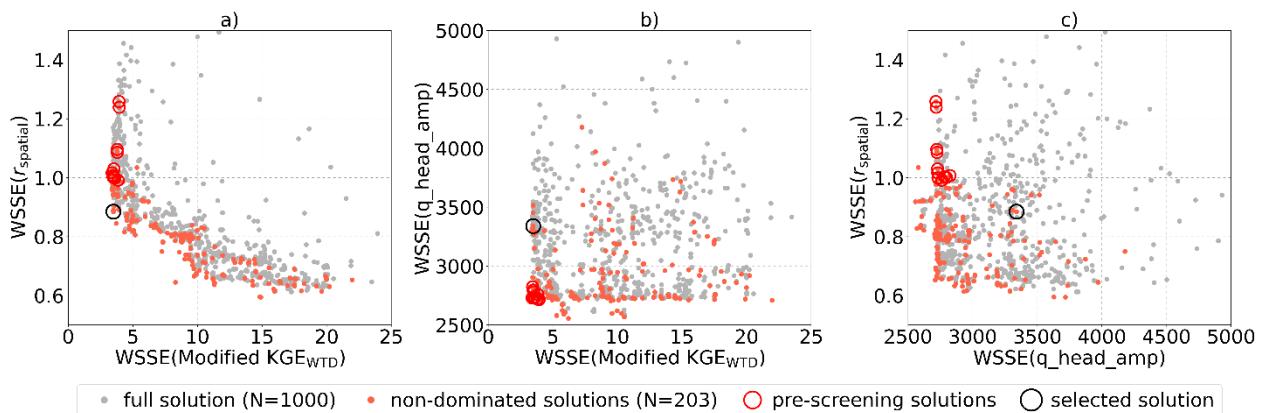
Figure 2: Scatterplots of WSSE (weighted sum of squared errors) for the three objective function groups in the calibration. Pareto front for 1000 model evaluations.

Hydrological model performance

Model performance metrics for the selected solution are summarized in Table 2. The q_head_amp objective function is separated into individual contributions from the metrics KGE_q, ME_{head} and ME_{amp}. Additionally, Table 2 shows the three metrics which make up the modified KGE_{wtd}: r_{wtd}, α_{wtd} and ME_{wtd}. In general, the model performs well with a KGE_{wtd} in peat of 0.64, a KGE_q of 0.63, a ME_{head} for the deep wells of 0.75 m and a ME_{amp} for the deep wells of 0.51 m for the selected solution. However, the correlation coefficient for the spatial variability ($r_{spatial}$) is poor with a value of 0.06. The model optimization achieves solid metrics on all the three components of KGE_{wtd}. The mean bias of WTD across all shallow peatland observation wells (ME_{wtd}) is only 8 cm (Table 2).

363 *Table 2: Hydrological model performance*

Name of metric		Abbreviation	Unit	Selected solution
Modified KGE on WTD		$KGE_{WTD_{modified}}$	-	0.64
	Correlation coefficient WTD	r_{WTD}	-	0.83
	Measure of variance	α_{WTD}	-	0.14
	Mean error of WTD	ME_{WTD}	m	0.08
Spatial correlation of the mean WTD		$r_{spatial}$	-	0.06
KGE on discharge		KGE_q	-	0.63
Mean error on the hydraulic heads		ME_{head}	m	0.75
Mean error on amplitude of the hydraulic heads		ME_{amp}	m	0.51

364

365 Though the model obtains a relatively small mean error, it largely underestimates the spatial variability
366 in WTD. The observed mean WTD variability across the 22 monitoring wells (SD = 16.5 cm) is
367 considerably higher than that observed in the simulations (SD = 6.8 cm). Even though the model
368 performance on KGE_{WTD} was generally good, it proved difficult to reproduce the spatial variation in
369 mean WTD.

370 To investigate the underestimation of spatial variability in WTD, we analyzed several spatial variables
371 considered relevant for explaining the observed variability in WTD: peat thickness, topography and
372 proximity to water bodies. However, no clear correlation was found between these spatial variables
373 and the mean observed WTD or model bias, as all had a correlation coefficient smaller than 0.34. See
374 Table S6.

375 Historical simulations of water table depth
376 The simulated WTD, generated by the calibrated hydrological model driven by historical climate for the
377 period 1990-2023, adequately represent both the observed seasonal patterns of WTD and their short-
378 term responses to precipitation events. Figure 3 shows the time series of WTD from two individual
379 monitoring wells as a typical example of the temporal match between observed and simulated WTD.
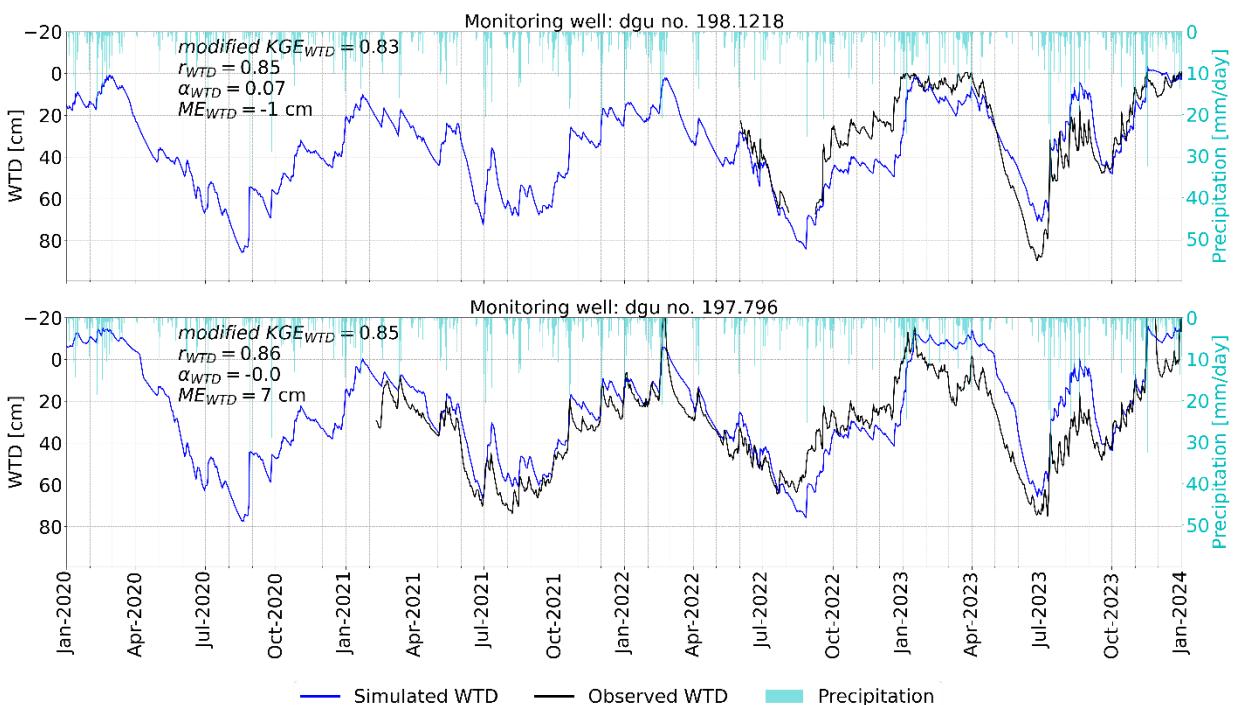
380

381 *Figure 3: Example of observed and simulated timeseries for water table depth (WTD) for monitoring wells dgu no. 198.1218*
382 *and dgu no. 197.796. Including metrics for these wells.*

Meteorological climate predictions

Changes in precipitation, temperature and evapotranspiration patterns in future climate projections for Denmark generally indicate an increase in both temperature and annual precipitation. Table 3 presents the mean air temperature, mean annual precipitation and mean potential evapotranspiration derived from the 17 climate projections across the three simulation periods.

Table 3: Mean ± SD (n=17) of annual air temperature, precipitation and potential evapotranspiration from the 17 climate models during the three simulation periods.

	Unit	Reference period (1991-2020)	Mid-century period (2041-2070)	End-of-century period (2071-2100)
Mean annual air temperature	∘C	8.9 ± 0.7	10.6 ± 0.8	12.1 ± 0.8
Mean annual precipitation	mm yr^{-1}	780 ± 121	837 ± 130	906 ± 152
Mean annual potential evapotranspiration	mm yr^{-1}	621 ± 25	678 ± 27	727 ± 27

Hydrological climate predictions

Climate simulations using the hydrological model indicate a decreasing trend in mean annual WTDs (Table 4), resulting in a shallower annual mean groundwater table in future climate conditions. Both summer and winter mean WTDs are projected to be closer to the surface, suggesting generally wetter conditions. The mean annual amplitude of WTD remains unchanged under future climate scenarios (Table 4), indicating that there is no greater seasonal drawdown of the water table during summer, although the duration of the drawdown period may be extended.

Table 4: Statistics of WTD when using the hydrological model for climate simulations. Mean ± SD (n=17) over the 17 climate models during the three simulation periods. Summer is June, July and August, Winter is December, January and February. The amplitude is based on the monthly means of WTD to avoid outliers.

	Unit	Reference period (1991-2020)	Mid-century period (2041-2070)	End -of-century period (2071-2100)
Mean annual WTD	cm	31 ± 1	27 ± 2	24 ± 3
Mean summer WTD	cm	47 ± 1	40 ± 3	34 ± 3
Mean winter WTD	cm	18 ± 2	14 ± 4	10 ± 3
Mean annual WTD amplitude	cm	51 ± 2	50 ± 4	52 ± 4

Derivation of empirical daily soil CO_2 flux model

An analysis of the Vejrumbro dataset indicated a clear temperature dependency on the relation between soil CO_2 flux (fCO_2) and WTD. The Vejrumbro dataset was resampled to daily means of WTD, T_{air} and soil CO_2 flux across the six spatial replicate measurement points omitting data from days with less than 24 flux measurements. This resulted in a dataset with 231 daily observations for each of fCO_2, WTD and T_{air} distributed evenly over a year. Traditionally, empirical emission models for ecosystem respiration (R_{eco}) are fitted to soil temperature. However, due to the strong linear relationship between daily soil temperature and daily air temperature at the Vejrumbro site (r = 0.96, p-value < 0.001) (Figure S4), T_{air} was used as a proxy for soil temperature when fitting the *Daily WTD-T_{air} model.* This use of air temperature also facilitates upscaling and omits the need for projecting soil temperatures under climate change scenarios.

To investigate how the WTD-fCO_2 relation scales with temperature, we binned daily soil CO_2 flux into five temperature intervals: <4°C (n=39), 4-8°C (n=32), 8-12°C (n=52), 12-16°C (n=70) and >16°C (n=38) and applied a linear regression model (*y=ax*) with the intercept constrained at zero within each temperature bin. The regressions were constrained to pass through the origin, reflecting the

417 assumption that soil CO_2 flux is zero when the WTD is zero. Thereby, the relationship between fCO_2
418 and WTD within each temperature bin was modeled using a linear regression of the form:

419 $fCO_2 = a \cdot WTD$ [5]

420 where fCO_2 represents soil CO_2 flux [Mg CO_2-C ha^{-1} day^{-1}], a denotes the fitted slope and WTD is water
421 table depth [cm], with positive values indicating depths below the surface.

422 This analysis revealed an increasing slope, i.e. sensitivity of soil CO_2 flux to changes in WTD, with rising
423 temperature (Figure S5 and Figure 4a), indicating that the WTD- fCO_2 slope (a) can be modelled as a
424 linear function of temperature (T_{air}) (Figure 4b):

425 $a = b \cdot T_{air} + c$ [6]

426 Combining these relationships yields a simple model of the soil CO_2 flux:

427 $fCO_2 = b \cdot T_{air} \cdot WTD + c \cdot WTD$ [7]

428 where T_{air} [$\circ$C] is the temperature, b [Mg CO_2-C ha^{-1} day^{-1} cm^{-1} $\circ$C^{-1}] and c [Mg CO_2-C ha^{-1} day^{-1} cm^{-1}] are
429 empirical constants.
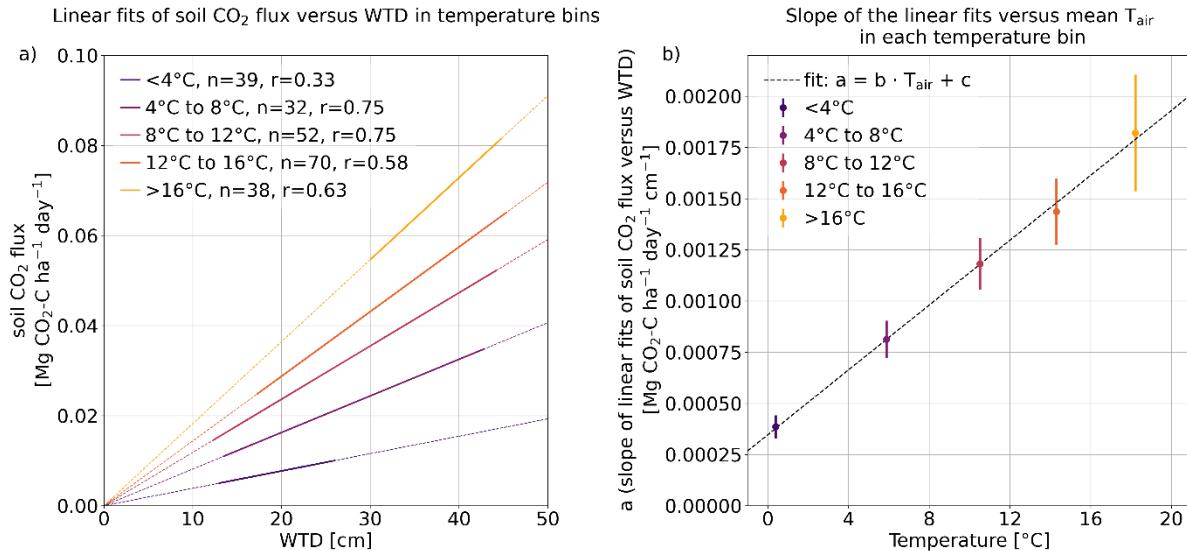
430

431 *Figure 4: Left: linear models of soil CO_2 flux vs. water table depth (WTD) in air temperature bins. The thicker segment of the*
432 *line represents the range of data used to derive the fitted model. n is the number of daily observations of soil CO_2 flux in each*
433 *temperature bin. r is Person correlation coefficient. Raw data behind the linear regressions can be seen at Figure S5. Right:*
434 *Slope (incl. uncertainty) (of the linear fit of soil CO_2 flux versus WTD) versus observed mean temperature in each temperature*
435 *bin.*

436 Having established a suitable form of the empirical soil CO_2 flux equation, we used nonlinear least
437 squares fit to estimate the b and c parameters based on the daily soil CO_2 flux, T_{air} and WTD (without
438 temperature bins). This method minimizes the residual sum of squares between the observed soil CO_2
439 flux and the *Daily WTD-T_{air} model*. The resulting fitted model demonstrated a significant correlation to
440 the observed data (r = 0.78, p-value < 0.001, RMSE = 0.021 Mg CO_2-C ha^{-1} day^{-1}) (Figure S6) with daily
441 soil CO_2 flux increasing in response to rising WTD and T_{air} (Figure S7). The fitted empirical constants are
442 as follows: b = 8.32$\cdot$10^{-5} Mg CO_2-C ha^{-1} day^{-1} cm^{-1} $\circ$C^{-1}, c = 3.33$\cdot$10^{-4} Mg CO_2-C ha^{-1} day^{-1} cm^{-1}.

443 The *Daily WTD-T_{air} model* predicts the highest soil CO_2 flux under conditions of simultaneously high T_{air}
444 and WTD, where a high WTD refers to a water table located furthest below the surface (dry
445 conditions). The multiplicative *Daily WTD-T_{air} model* demonstrated a moderate fit to the soil CO_2 flux
446 data, with a R^2 of 0.61. To assess the individual contributions of the predictor variables, we also

447   computed the R^2 between CO2 flux and T_{air} and WTD separately. This was done using a constructed

448   dataset that included all combinations of WTD and T_{air} within the model range. This resulted in R^2

449   values of 0.34 for T_{air} and 0.54 for WTD (Table S7). These values reflect the explanatory power of each

450   variable in isolation.

451   Despite the significant variability in the observed net ecosystem carbon balance (NECB) used for the

452   *Annual WTD model* (Figure 5) it is considered to represent a robust mean as it is based on multiple

453   sites and years for Danish and German conditions. Compared to the *Annual WTD model* both the

454   measured soil CO_2 flux (12.9 Mg CO_2-C ha^{-1} yr^{-1} (green circle)) and the *Daily WTD-T_{air}* simulated soil CO_2

455   flux (13.6 Mg CO_2-C ha^{-1} yr^{-1} (not shown)) at Vejrumbro are above the corresponding fitted value of

456   NECB (8.7 Mg CO_2-C ha^{-1} yr^{-1} (orange circle)) based on an annual WTD of 29 cm, but still within the

457   range of observed NEBCs used for fitting the *Annual WTD model* (Figure 5). This may be explained by

458   the methodology of flux measurements at Vejrumbro that did not consider GPP (CO_2 uptake) and

459   therefore are expected to result in higher net CO_2 fluxes. In order to align the *Daily WTD-T_{air} model* to

460   the level of the *Annual WTD model* where GPP is included, a scaling factor based on the above

461   differences ($f_{scaling}$ = 0.64) was applied to equation 7 to account for lack of GPP in the soil CO_2 fluxes

462   used for empirical model development. Applying this scaling factor, we seek to avoid the risk of

463   overestimating emissions when applying the *Daily WTD-T_{air} model* at other locations.

○   Danish flux data for fitting the *Annual WTD model*
·   German flux data
——   *Annual WTD model* (Koch et al, 2023)
●   Annual soil CO_2 flux measured at Vejrumbro
●   NECB at Vejrumbro calculated with the *Annual WTD model*
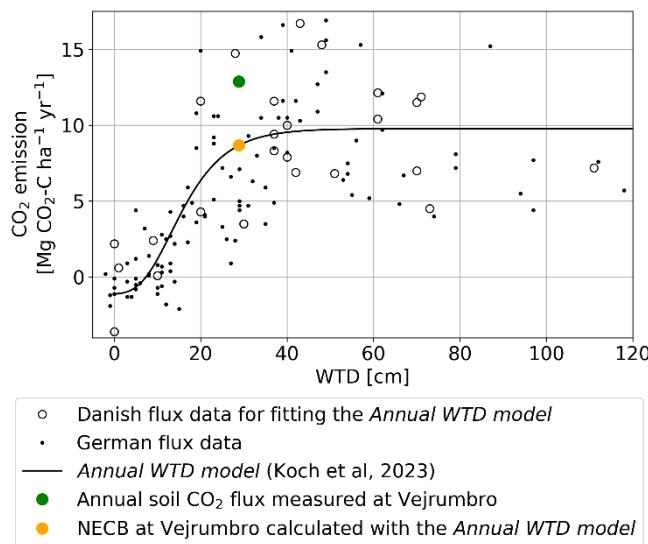
464

465   *Figure 5: The Annual WTD model together with the Danish flux data of annual NECB and WTD data underlaying the model*
466   *(Koch et al., 2023). German flux data are included for comparison (Tiemeyer et al., 2020). Colored circles are measured and*
467   *calculated soil CO_2 flux and NECB for the Vejrumbro dataset, so the colored circles represent the year 2022-2023.*

468   The Vejrumbro dataset used for fitting the *Daily WTD-T_{air} model* was limited to a maximum WTD of 47

469   cm and maximum T_{air} of 21°C (Figure S7). Outside this range, the predictions of the *Daily WTD-T_{air}*

470   *model* exhibits increased uncertainty. At the same time, it is generally understood that the upper

471   portion of the peat layer drives the net CO_2 emissions observed at the surface. Therefore, the

472   extrapolation of WTD in the *Daily WTD-T_{air} model* must be constrained. The *Daily WTD-T_{air} model*

473   should be sensitive within a WTD range comparable to the expected daily variation in the *Annual WTD*

474   *model*, which also reaches an fCO_2 asymptotic at deeper water tables. In the *Annual WTD model*, the

475   Annual NECB reaches 90% of its maximum asymptotic level at a mean annual WTD of 30 cm (Figure 5).

476   The mean annual WTD results from intra-annual (within year) WTD variation described by the annual

477   amplitude. The mean annual amplitude (based on monthly means) is 65 cm, across the 22 observed

478   WTD time series in the Tuse Stream catchment used for calibrating the hydrological model. We

479   assume that a mean annual WTD of 30 cm originates from an annual WTD variation with a similar

480 amplitude. Therefore, we assume that the WTD range of the *Daily WTD-T_{air} model* is 30 + 65/2 cm =
481 62.5 cm. For the T_{air} range, it is assumed that the sensitivity continues until 25°C, which is a daily
482 average value very rarely occurring, even in future climate projections. Thus, when applying the *Daily*
483 *WTD-T_{air} model,* daily WTD values and T_{air} values were truncated, setting WTD and T_{air} to 62.5 cm and
484 25°C, respectively, when exceeding those thresholds.

485 In both the *Daily WTD-T_{air} model* and *the Annual WTD model,* CO_2 fluxes are constrained so that the
486 model does not simulate negative fluxes or carbon uptake. ~~Thus, both CO_2 flux models exclusively~~
487 ~~account for the CO_2 emissions from the peat soil, without representing its potential role as a carbon~~
488 ~~sink~~ (Gyldenkærne et al., 2025).

CO_2 emissions from peatlands

CO_2 emissions throughout the historical simulation period

491 The long-term mean of the emission factor for the Tuse Stream catchment peat area is 8.0 ± 0.8 Mg
492 CO_2-C ha^{-1} yr^{-1} (mean ± SD, n=34) when using the *Annual WTD model* and 8.8 ± 1.6 Mg CO_2-C ha^{-1} yr^{-1}
493 (mean ± SD, n=34) when using the *Daily WTD-T_{air} model* (Table 5).

494 *Table 5: Long-term mean water table depth (WTD), long-term mean annual WTD amplitude (based on monthly means of WTD*
495 *to avoid outliers) and long-term soil CO_2 flux, throughout the historical period and the three modified 34-year WTD time series*
496 *of rewetting scenarios. Mean ± SD is based on the 34 years of the historical period (1990-2023).*

	Unit	Historical period (1990-2023)	Rewetting scenario A	Rewetting scenario B	Rewetting scenario C
Mean WTD	cm	34 ± 8	14 ± 18	14 ± 8	14 ± 4
Mean annual WTD amplitude	cm	51 ± 11	110 ± 28	51 ± 11	26 ± 5
CO_2 emission from *Daily WTD-T_{air} model* aggregated to annual	Mg CO_2-C ha^{-1} yr^{-1}	8.8 ± 1.6	7.7 ± 2.0	5.2 ± 1.5	4.4 ± 0.8
CO_2 emission from *Annual WTD model* aggregated to annual	Mg CO_2-C ha^{-1} yr^{-1}	8.0 ± 0.8	4.6 ± 3.0	4.3 ± 2.0	4.4 ± 1.2

497

498 Figure 6 shows T_{air}, as wells as the spatial mean of WTD and CO_2 emissions across the peatland, as
499 simulated by the *Daily WTD-T_{air} model* and the *Annual WTD model* during the historical period. The
500 CO_2 emissions calculated with the *Daily WTD-T_{air} model* (red line in Figure 6c, 6d) depend on both the
501 observed daily temperature variability (orange line in Figure 6a) and simulated intra-annual (seasonal)
502 WTD variability (blue line in Figure 6b), while the CO_2 emission calculated with the *Annual WTD model*
503 (black points in Figure 6d) only depends on the inter-annual (annual means) WTD (blue points in Figure
504 6b) and not the temperature.

505 Inter-annual (between years) variation in CO_2 emission is substantially larger when using the *Daily*
506 *WTD-T_{air} model* (SD = 1.6 Mg C-CO_2 ha^{-1} yr^{-1}) compared to the *Annual WTD model* (SD = 0.8 Mg C-CO_2
507 ha^{-1} yr^{-1}) (Figure 6d), as the former captures extreme events, such as periods of high temperature or
508 deep groundwater tables, as well as compound events involving the simultaneous occurrence of both.
509 In contrast, the *Annual WTD model* is insensitive to temperature and the intra-annual (within year)
510 timing of deep WTD. Moreover, the *Annual WTD model* imposes an upper limit of 10 Mg CO_2-C ha^{-1}
511 yr^{-1} for annual emissions (Koch et al., 2023) (Figure 5). During the summer of 2018, a compound
512 extreme event occurred, characterized by both high temperatures and deep groundwater table. The
513 annual CO_2 flux for this year shows a 34% increase when estimated using the *Daily WTD-T_{air} model*
514 compared to the *Annual WTD model*. This discrepancy arises from the *Daily WTD-T_{air} model's* ability to
515 account for the prolonged duration of concurrent high temperatures and deep groundwater table
516 conditions throughout the summer (Figure 6d). Conversely, in 2010, the *Daily WTD-T_{air} model*
517 estimates significantly lower annual CO_2 emissions compared to the *Annual WTD model* (Figure 6d).

518   This difference is due to the emission model's ability to account for the effects of prolonged periods of
519   low temperatures during the autumn and spring of 2010, leading to a mean annual temperature below
520   the long-term mean, despite summer temperatures being consistent with other years (Figure 6a).
521   Examples of years with extreme events primarily driven by either WTD or T_{air} include 1996, which
522   experienced a significant summer decline in groundwater table (Figure 6b), and 1997, which was
523   characterized by elevated summer temperatures (Figure 6a). However, neither of these events led to
524   CO_2 emissions as high as those simulated during the compound event of both high temperatures and
525   deep water table in 2018 (Figure 6).
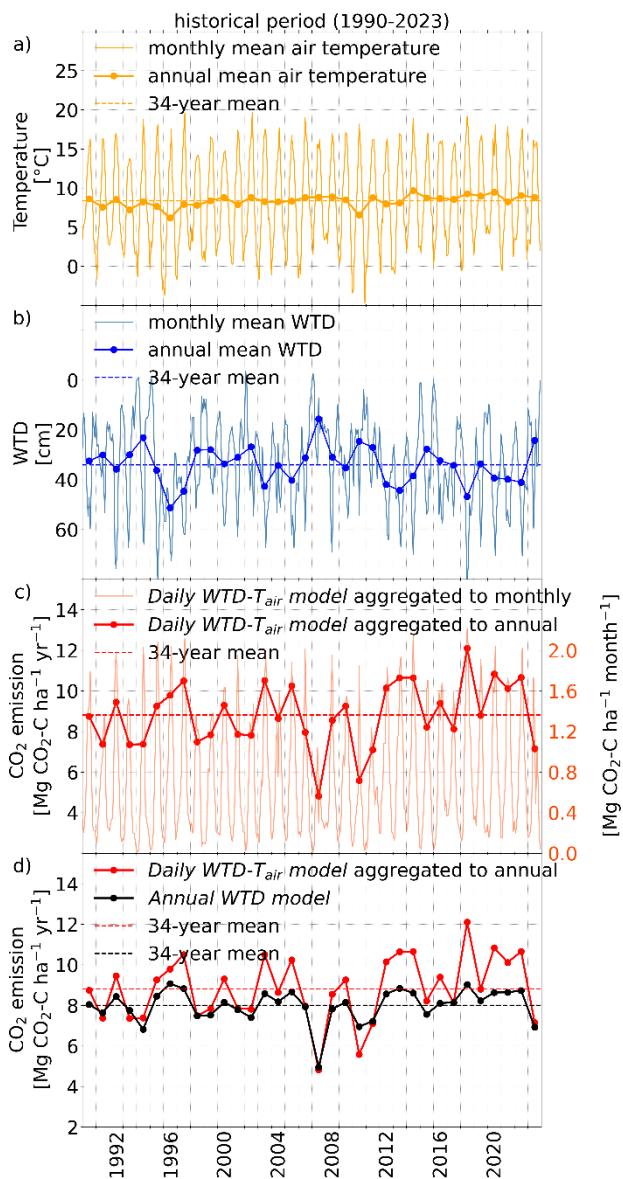
526

527   *Figure 6: Air temperature (T_{air}), water table depth (WTD) and soil CO_2 emission for the historical simulation period 1990-2023.*

528   CO_2 emissions under different rewetting scenarios
529   The rewetting scenarios represent an adjustment to the WTD simulated by the hydrological model
530   over the 34-year historical period, thereby reflecting the climatological conditions prevailing during
531   that time. Across all three rewetting scenarios, the long-term (34-year) mean WTD was raised by 20
532   cm, from 34 cm to 14 cm below the surface, ensuring a consistent long-term annual mean WTD among
533   the rewetting scenarios (Table 5). Accordingly, the application of the *Annual WTD model* for estimating
534   CO_2 fluxes result in CO_2 emissions between 4.3 ± 1.2 Mg C-CO_2 ha^{-1} yr^{-1} (mean ± SD, n=34) and 4.6 ± 3.0

535 Mg C-CO$_2$ ha^{-1} yr^{-1} (mean ± SD, n=34) across all rewetting scenarios (Table 5). The mean annual soil CO$_2$
536 flux from the three rewetting scenarios, as calculated using the *Annual WTD model,* are similar but not
537 identical. This is because the *Annual WTD model* is applied to each of the 34 individual annual mean
538 WTD values rather than to a single long-term mean WTD. The SD of CO$_2$ emissions calculated using the
539 *Annual WTD model* in scenario C is markedly lower than in rewetting scenario A and B, reflecting the
540 lower inter-annual (between years) variability in mean annual WTD observed for this scenario (Table
541 5).

542 In contrast to the *Annual WTD model*, the *Daily WTD-T$_{air}$ model* captures the simultaneous occurrence
543 of low groundwater table and high T$_{air}$ during the summer months. Application of this emission model
544 indicates that raising the groundwater table during summer months (rewetting scenario C) yields the
545 greatest reduction potential in soil CO$_2$ emissions (Table 5), leading to a 50% decrease in the mean
546 value, from 8.8 ± 1.6 to 4.4 ± 0.8 Mg C-CO$_2$ ha^{-1} yr^{-1} (mean ± SD, n=34) (Table 5). In contrast,
547 management scenarios that primarily target increase in winter water table (rewetting scenario A)
548 exhibit only marginal emission reduction potential (Table 5).

549 A visual representation of daily soil CO$_2$ emissions in relation to mean daily temperature during the 34-
550 year historical period under different WTD conditions (Figure 7) reveals that high summer
551 temperatures are a key driver of CO$_2$ emissions. WTD observations from the Tuse catchment peatland
552 indicate that, during shorter periods in the warm summer months, the WTD can exceed 80 cm (Figure
553 3). These periods with very low summer water table contribute substantially to total CO$_2$ emissions
554 (Figure 7).

555 A rewetting scenario that mainly generates wetter winter conditions (rewetting scenario A) has very
556 limited CO$_2$ emission reduction. All three scenarios assume that even under rewetting, the peatland
557 WTD will follow a climate driven seasonality and that obtaining zero WTD in summer periods will be
558 difficult by classical nature-based solutions. Rewetting scenario C, which features the greatest increase
559 in summer WTD, achieves the largest reduction in CO$_2$ emissions (Figure 7). Permanent wet conditions
560 with WTD at zero would be required to obtain zero CO$_2$ emission with the developed *Daily WTD-T$_{air}$
561 model,* but under such conditions, methane emissions would also come into play and plant growth
562 would be severely limited.
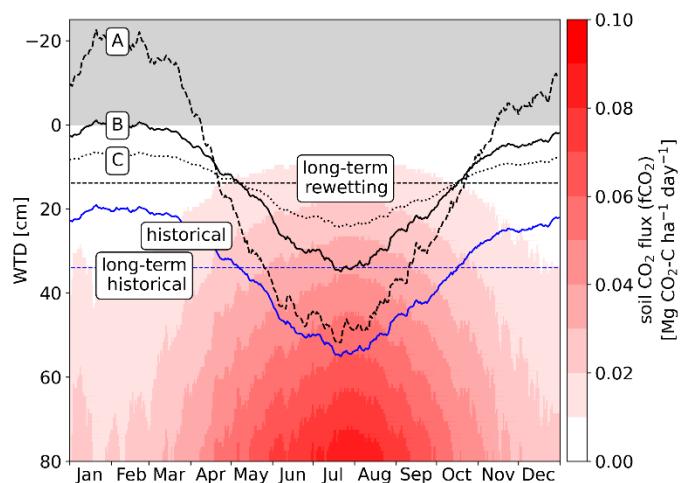
563

564 *Figure 7: Colormap: Visual representation of the annual distribution of daily surface soil CO$_2$ flux (fCO$_2$, CO$_2$ exchange with*
565 *atmosphere) under mean daily temperature during the historical period (1990-2023) and for different water table depths*
566 *(WTD). Curves: solid blue line: simulated daily mean WTD during the historical period and corresponding long-term (34-year)*
567 *mean WTD, black lines: daily mean WTD for each of the modified 34-year WTD time series of rewetting scenarios (A, B and C)*
568 *and the corresponding long-term (34-year) mean WTD.*

569   CO_2 emissions across future climate simulation periods
570   Figure 8 shows the same variables as Figure 6 but based on a representative climate model simulation
571   instead of the observed climate record, offering a typical example of the development of temperature,
572   WTD and soil CO_2 flux through the reference, mid-century and end-of-century periods based on the
573   RCP 8.5 pathway.

574   The future climate simulations show an increase in both the annual mean temperature and
575   groundwater levels combined with higher maximum summer temperature (Figure 8a, 8b, Table 3,
576   Table 4). The bootstrap mean of soil CO_2 flux calculated with the *Annual WTD model* over all climate
577   models predicts a decreasing trend in soil CO_2 flux under future climate conditions (Figure 9a,
578   horizontal dotted black line in Figure 8d), driven by an inter-annual (between years) mean WTD closer
579   to surface (Table 4, Figure 8b). However, this decreasing trend is countered by the inclusion of T_{air}
580   effects when applying the *Daily WTD-T_{air} model* (Figure 9b, horizontal dotted red line in Figure 8c and
581   8d).

582   The wider confidence intervals in the mean annual CO_2 emissions for the future periods with both CO_2
583   emission model (Figure 9) indicate that the inter-annual (between years) soil CO_2 fluxes become more
584   variable in future climate. Furthermore, the confidence intervals for the individual periods are wider
585   for the *Daily WTD-T_{air}* (Figure 9b) compared to the *Annual WTD model* (Figure 9a), which is expected as
586   variations in T_{air} and not only WTD is included as with the *Daily WTD-T_{air} model*. This demonstrates that
587   the *Daily WTD-T_{air} model* captures extreme events, including periods of high temperature or deep
588   groundwater table, whether these events occur simultaneously (compound event) or independently.

589
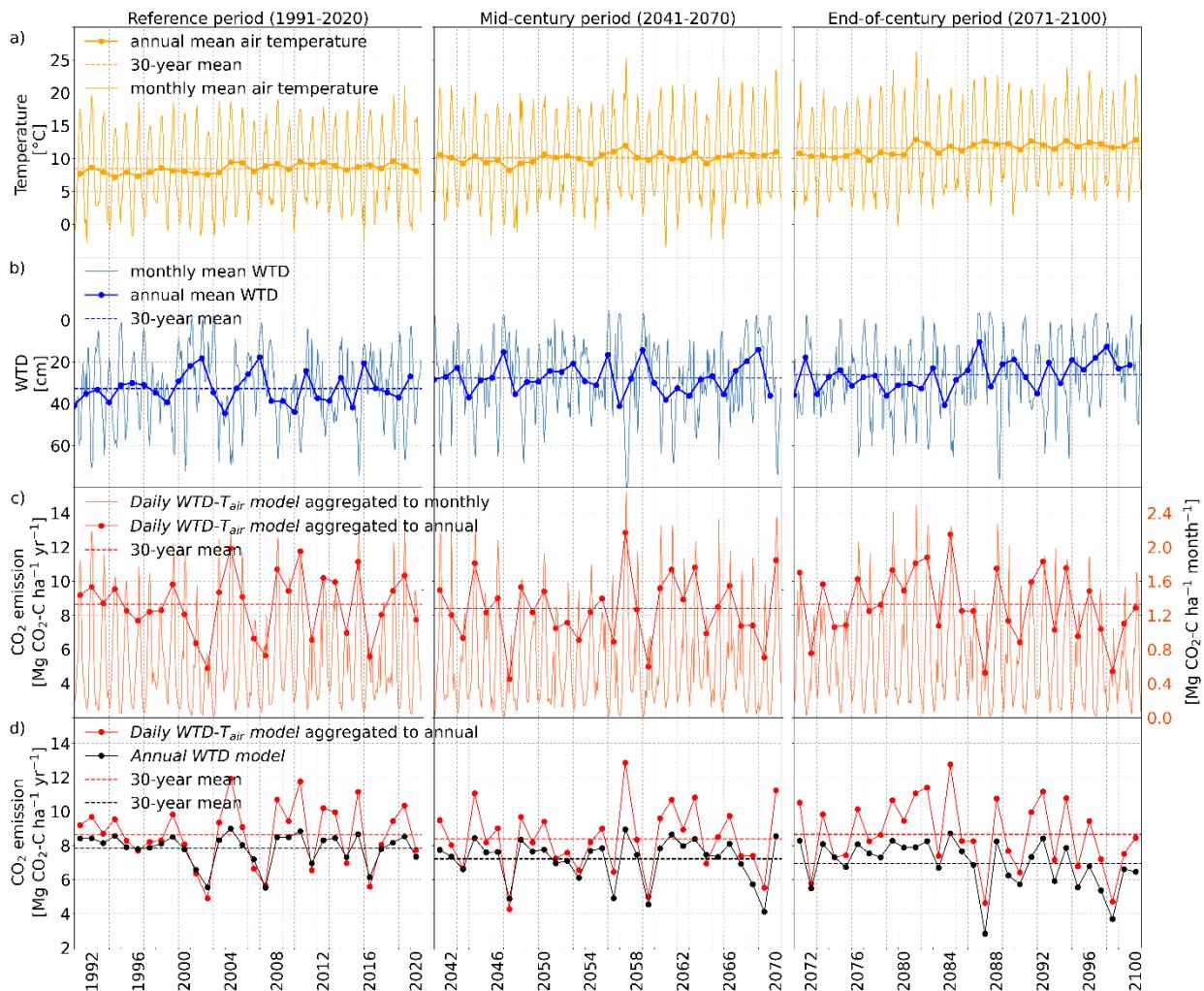
590 *Figure 8: Example of air temperature (T$_{air}$), water table depth (WTD) and soil CO$_2$ flux for future climate simulation with*
591 *climate model projection no. 5 (Table S6).*

592
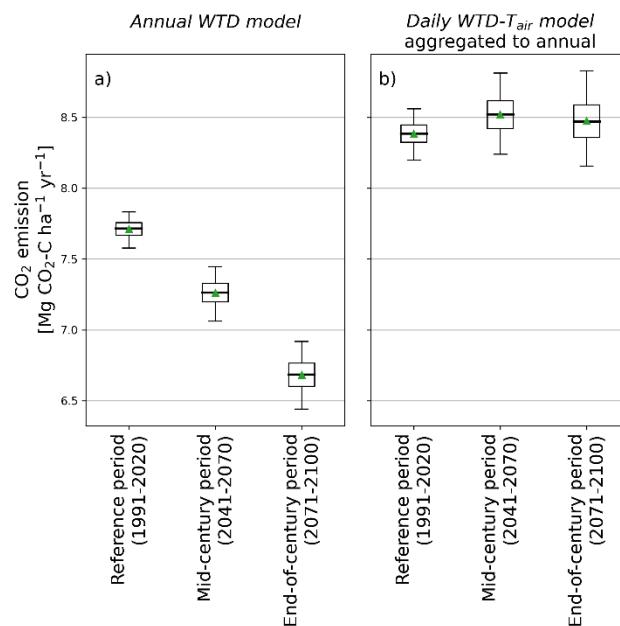
593 *Figure 9: Boxplot showing the distribution of bootstrap means of soil CO$_2$ emissions according to the Daily WTD-T$_{air}$ model and*
594 *Annual WTD model during future climate. Green triangles and horizontal lines indicate the mean and the median of the*

597 The results presented in Figure 9 suggest that the impact on CO_2 emissions caused by future increases
598 in T_{air} and increases in water tables cancel each other out when using the *Daily WTD-T_{air} model*. To
599 investigate this further, we analyze how the combination of T_{air} and WTD shift between the reference
600 and the end-of-century periods, despite relatively stable total CO_2 emission.

601 We wish to identify the specific combination of T_{air} and WTD that are associated with the majority of
602 the CO_2 emission. Due to the non-linear response of soil CO_2 flux to environmental drivers in the *Daily*
603 *WTD-T_{air} model*, a large fraction of total emissions is generated on relatively few days. To quantify this,
604 we calculated p50, defined as the proportion of days required to account for 50% of the total annual
605 soil CO_2 flux (fCO2). This was achieved by ranking the daily values of fCO2, WTD, and T_{air} in ascending
606 order according to fCO2. Subsequently, the ranked fCO2 values were cumulatively summed to obtain
607 their percentile distribution (Figure S8). The procedure was first applied to fCO2, WTD, and Tair data
608 from the historical simulation period, with the resulting percentile curves shown in Figure S8. Over the
609 historical simulation period, 50% of the total fCO2 ($fCO_{2, p50}$) was generated within 22% of the days (p50
610 = 22%), while the value of $fCO_{2, p50}$ and corresponding WTD_{p50} and $T_{air, p50}$ are estimated to be $4.15 \cdot 10^{-2}$
611 g CO_2-C ha^{-1} day^{-1}, 47 cm and 13.8 °C (Table 6 and Figure S8).

612 Similar estimates are derived from the three timeslots from the climate models (reference, mid-
613 century and end-of-century climate simulation periods) using the 17 different climate models. For the
614 future, 50% of the total fCO2 is expected to occur within approximately 21 ± 1 % (mean ± SD, n=17) of
615 the days (Table 6). The daily soil CO_2 flux associated to p50 ($fCO_{2, p50}$) and p50 are nearly identical
616 across both the historical and future climate simulations periods (Table 6). As also shown in Figure 9b,
617 the magnitude and temporal distribution of fCO2 are predicted to remain unchanged in the future.
618 While the value of $fCO_{2, p50}$ remains relatively constant around $4 \cdot 10^{-2}$ Mg CO_2-C ha^{-1} day^{-1} for future
619 climate periods, the corresponding WTD_{p50} and $T_{air, p50}$ values change as a result of changing climate
620 moving towards higher temperatures (17 °C) and shallower groundwater table (40 cm).

621 Figure 10 provides a graphical representation of fCO2 obtained from the *Daily WTD-T_{air} model*, with the
622 colormap illustrating the daily fCO2 corresponding to different combinations of T_{air} and WTD. The daily
623 $fCO_{2, p50}$ ($4.15 \cdot 10^{-2}$ g CO_2-C ha^{-1} day^{-1} for the historical period (Table 6)) can be achieved through
624 various combinations of T_{air} and WTD (dark red dotted line in Figure 10). The values of $T_{air, p50}$ and
625 WTD_{p50} corresponding to $fCO_{2, p50}$ for the Tuse Stream catchment peatland are plotted as a dark red
626 point. As expected, the $fCO_{2, p50}$ values for the reference periods of the 17 climate models (green
627 crosses at Figure 10) are closely aligned with that of the historical period. It is evident that the $fCO_{2, p50}$
628 values for the end-of-century climate conditions (blue crosses at Figure 10) shift along the direction
629 indicated by the pink arrow (along the red dotted line), reflecting a trend toward higher temperatures
630 and lower WTD (i.e. water levels closer to the surface surface). This indicates that the mean daily fCO2
631 (Table 6) and the long-term fCO2 remains constant in the future (Figure 9b), as a result of a
632 counterbalance between impacts of rising temperatures and rising groundwater levels.

633 The pink arrow at Figure 10 illustrates the characteristic impact of climate change in Denmark,
634 reflecting the concurrent increase in air temperature and shallow groundwater levels (Schneider et al.,
635 2022). In contrast, other regions in Europe are experiencing declining groundwater level trends to
636 climate change (Wunsch et al., 2022). Consequently, CO_2 emissions from peatlands in these regions
637 are expected to shift in the direction indicated by the yellow arrow in Figure 10, towards considerably
638 larger emission rates.

639 *Table 6: p50 is the fraction of days required to reach 50% of the total soil CO$_2$ flux (fCO$_2$). fCO$_{2, p50}$ is the daily soil CO$_2$ flux*
640 *associated with p50. WTD$_{p50}$ and T$_{air, p50}$ are the water table depth (WTD) and air temperature (T$_{air}$) corresponding to fCO$_{2, p50}$,*
641 *respectively. Mean ± SD is based on 17 climate model simulations.*

		Historical simulation period	Climate simulation periods		
	Unit	(1990-2023)	Reference period (1991-2020)	Mid-century period (2041-2070)	End-of-century period (2071-2100)
p50	% days	22	21 ± 1	21 ± 1	21 ± 1
fCO$_{2, p50}$	Mg CO$_2$-C ha^{-1} day^{-1}	$4.15 \cdot 10^{-2}$	$4.03 \cdot 10^{-2} \pm 9.89 \cdot 10^{-4}$	$4.00 \cdot 10^{-2} \pm 3.24 \cdot 10^{-3}$	$4.03 \cdot 10^{-2} \pm 3.65 \cdot 10^{-3}$
T$_{air, p50}$	°C	13.8	14 ± 0.3	15 ± 0.6	17 ± 1.0
WTD$_{p50}$	cm	47	46 ± 1	42 ± 3	40 ± 3

642
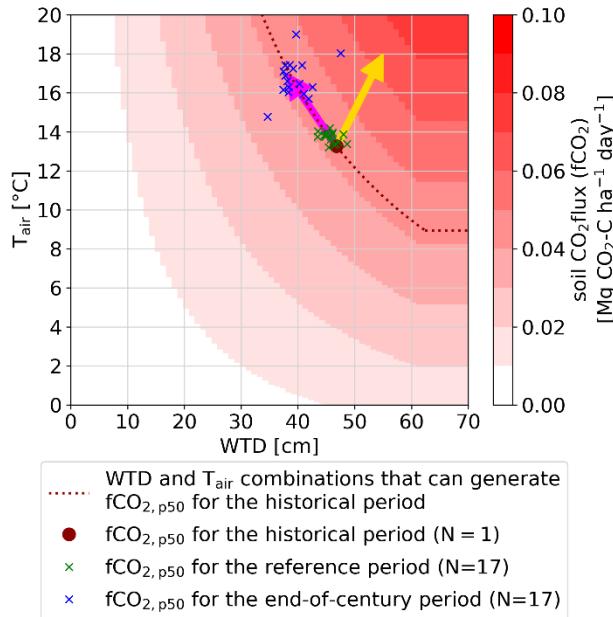
643

644 *Figure 10: Colormap: Visual representation of the Daily WTD-T$_{air}$ model output, illustrating soil CO$_2$ flux (fCO2) as function of*
645 *daily water table depth (WTD) and air temperature (T$_{air}$). The dark red dotted line represents combinations of T$_{air}$ and WTD*
646 *that corresponds fCO$_2$ at p50 (fCO$_{2, p50}$), where p50 is the fraction of days required to reach 50% of the total accumulated fCO$_2$*
647 *during the historical period. Green crosses are fCO$_{2, p50}$ for the reference period of the 17 climate simulations. Purple crosses*
648 *are fCO$_{2, p50}$ for the end-of-century climate simulation period of the 17 climate simulations. The pink and yellow arrows*
649 *indicate different future trends in T$_{air}$ and WTD and the associated trend in CO$_2$ emissions under climate change. Specific to*
650 *Denmark, the pink arrow indicates increases in T$_{air}$ and decrease in WTD, other regions might experience increase in both T$_{air}$*
651 *and WTD and an associated large increase in CO$_2$ emissions (yellow arrow).*

Discussion

Peatland management under changing climate

In 2023, CO_2 emissions from drained organic soils in croplands and grasslands was estimated to have accounted for 6.7% of Denmark's total emissions, including those from the Land Use, Land-Use Change and Forestry (LULUCF) sector (Nielsen et al., 2025b). Returning peatland organic soils to their natural hydrological state is a cost-effective GHG reduction strategy (IPCC, 2014; Kirpotin et al., 2021; Tanneberger et al., 2021; Wilson et al., 2016). Therefore, national policies (Regeringen, 2024) and the European Union's Nature Restoration Law (Regulation (EU) 2024/1991, 2024) seek to improve the management of peatlands and achieve climate neutrality targets under the urgent Green Transition agenda. To mitigate agricultural GHG emissions Danish ministerial agreements were initiated in 2024, targeting the restoration of 140,000 hectares of peatland (Regeringen, 2024). However, there is a need to strengthen the scientific evidence for mitigation measures to facilitate cost-effective policies. Quantitative predictions of fluxes such as the numbers presented in this study, supports prioritization and design of peatland rewetting strategies by estimating their CO_2 emission reduction potentials accounting for future climate variability impact on CO_2 emissions.

Integration of the process-based hydrological model of the Tuse Stream catchment with the empirically derived *Daily WTD-T$_{air}$ model* of soil CO_2 flux developed in this study revealed that emission simulations at daily timesteps produce greater variability in soil CO_2 fluxes compared to emission estimates derived from annual WTD means. This increased variability is attributed to the daily model's ability to account for short-term compound events, especially the simultaneous occurrence of elevated air temperatures and low groundwater levels.

More importantly, incorporating temperature dependence and higher temporal resolution into the CO_2 emissions model significantly alters the projected trends of CO_2 emission under both rewetting and changing climate conditions.

Nature-based approaches represent the most common real-world rewetting strategies, aiming to restore peatlands towards their natural hydrological regime. At a minimum, such rewetting requires terminating tillage activities and eliminating artificial drainage for instance by blocking of drainpipes and ditches. The rewetting scenarios implemented in this study, represented as simple modifications to WTD, are not reflective of practical management interventions - except perhaps in a few rare and costly restoration projects that involve installing artificial impermeable membranes along peatlands edges (Naturstyrelsen, 2022). However, the outcome of this study can serve as a reference for discussions on realistic expectations on CO_2 emission reductions from rewetted peatlands.

The rewetting analyzed in this study showed how different rewetting scenarios with varying seasonal amplitudes in WTD suggest significantly different emission reduction potential even with identical annual mean WTD. The results illustrate that increasing the groundwater table during warm periods is key to obtaining CO_2 emission reductions, whereas rewetting strategies that mainly raise winter water table without significantly affecting the summer levels offer limited mitigation benefits. This highlights the importance of not only targeting annual reductions in WTD but particularly designing rewetting strategies to increase the summer water table and avoid critically low water levels during droughts and warm periods. Achieving such rewetted conditions may include larger forced control of WTD than what is currently being practiced for most existing rewetting schemes, where the WTD remain subject to climate seasonality impact. Such nature-based solutions are not likely to reduce CO_2 emissions to the degree that current emission reduction policies target.

696 Also, projections of CO_2 emissions under different climate change scenarios were altered greatly by
697 introducing temperature sensitivity and enhanced temporal resolution into the CO_2 emissions
698 modeling framework. Here our results show that, while the projected rise in groundwater tables in
699 isolation would lead to lower CO_2 emissions in future (when using the *Annual WTD model*), the *Daily*
700 *WTD-T_{air} model* revealed that anticipated increases in T_{air} are likely to cancel out these reductions,
701 resulting in CO_2 emissions on a level comparable to current levels. This is an important finding, since it
702 suggests that increasing temperatures alone will likely increase CO_2 emissions, and that water level rise
703 driven by climate change or rewetting initiatives might just counteract this trend. Rewetting measures
704 would need to be substantially intensified to ensure climate resilience and achieve meaningful
705 reductions in CO_2 emissions. Additionally, outside the specific case of Danish peatlands located in a
706 region that is susceptible to a future wetter climate, other regions might project both increasing
707 temperatures and lower groundwater tables, and in such cases climate change will significantly
708 increase emissions without any rewetting. We acknowledge that the chosen Representative
709 Concentration Pathway (RCP8.5) represents the scenario leading to the strongest impact of climate
710 change and that additional, milder climate scenarios could have been included.

711 Hydrological simulation of groundwater levels in peat soil with process-based models
712 Existing large scale CO_2 emission estimates, such as national inventories from organic soils
713 (Gyldenkærne et al., 2025; Nielsen et al., 2025b), typically combine empirical emission models and
714 data-driven ML approaches for estimating annual WTD (Bechtold et al., 2014; Koch et al., 2023;
715 Tiemeyer et al., 2020). These approaches appear robust and suited for upscaling but are limited in
716 their ability to represent the impact of sub-annual variability in temperature and WTD, which are
717 issues that become increasingly important when analyzing effects of rewetting and climate change. In
718 contrast to most data-driven approaches, hydrological models enable a climate-driven representation
719 of WTD temporal dynamics and the underlying hydrological processes. Moreover, the use of physically
720 based hydrological models has the distinct advantage of enabling scenario-based analyses, such as the
721 evaluation of alternative land use strategies and the projection of future hydrological conditions under
722 climate change scenarios. Utilizing hydrological models that generate high-resolution time series of
723 WTD, it is possible to quantify impacts of WTD dynamics, including water levels, temporal variability
724 and seasonal amplitudes, on changes in CO_2 emissions.

725 That said we acknowledge that the rewetting scenarios in the present study are applied using
726 simplified adjustments to the simulated WTD, rather than being modeled through a detailed, process-
727 based hydrological framework. Ideally, future assessments should apply catchment-scale models to
728 evaluate peatland management interventions, such as rewetting, thereby enabling analysis of their
729 broader hydrological impacts, including effects on streamflow and groundwater levels in neighboring
730 areas.

731 A unique feature of the present study is that the hydrological model of Tuse Stream catchment is
732 developed in the same modelling framework as the National Hydrological Model of Denmark
733 (Henriksen et al., 2020; Stisen et al., 2019). The National Hydrological Model is continuously updated
734 with new data and operates in near real-time. This integration enables a link between the lessons
735 learned from the Tuse Stream catchment-scale model and the National Hydrological Model of
736 Denmark, thereby improving the representation of peatland hydrology and contributing to the
737 refinement of future national GHG inventories.

738 As a continuation of this study, we will further investigate the spatial variability of WTD and extent
739 hydrological model to include additional peatland-dominated catchments. Additionally, we will utilize
740 the National Hydrological model to simulate WTD across all Danish peatlands.

741 Selection, fit and transferability of daily CO_2 emission model

742 Detailed process-based terrestrial ecosystem models that simulate biogeochemical cycles and
743 vegetation are available (Bona et al., 2020; Oikawa et al., 2017; Wu and Blodau, 2013). Such modelling
744 schemes rely largely on multiple parameters related to plant and soil biogeochemistry which are not
745 generally attainable, thereby limiting the possibility to generalize and upscale.

746 As an alternative a range of empirical models with varying levels of complexity has been developed to
747 describe ecosystem respiration; however, the most commonly applied formulation is the Lloyd–Taylor
748 model (Lloyd J., Taylor, 1994), in which temperature acts as the sole independent variable. Structural
749 complexity in empirical equations is increased through the integration of various other environmental
750 variables, for example, hydrological variables such as WTD (Rigney et al., 2018). Recent alternative
751 empirical approaches for estimating CO_2 emissions for organics soils include response functions linking
752 average annual WTD to annual emissions (Arents et al., 2018; Evans et al., 2021; Tiemeyer et al., 2020),
753 such as the *Annual WTD model* (Koch et al., 2023) used in this study.

754 To evaluate alternative empirical emission models alongside our *Daily WTD-T_{air} model,* we fitted three
755 different empirical formulations from Rigney et al. (2018) to the Vejrumbro soil CO_2 flux data (Table
756 S7). Each of the three empirical formulations incorporated both temperature and WTD as independent
757 variable. The model fitting resulted in R^2 values comparable to those obtained from fitting the *Daily*
758 *WTD-T_{air} model* developed in this study (Table S7).

759 Studying the explanatory power of each independent variable of WTD and T_{air} in isolation in the other
760 empirical emission models, revealed that models in which WTD and T_{air} are incorporated as additive
761 terms, rather than as interdependent (e.g., multiplicative) terms (as in eq. 6 and 8 in Rigney et al.,
762 (2018)), often exhibit coefficients of determination (R^2) that are excessively dominated by either WTD
763 or T_{air} (Table S7). This indicates that such model formulations may inadequately capture the joint or
764 synergistic effects of these variables on the dependent variable. The challenge likely stems from the
765 fact that both WTD and T_{air} exhibit similar seasonal patterns, which may lead the regression to
766 primarily fit one of the additive terms containing either WTD or T_{air}. Empirical models that incorporate
767 WTD and T_{air} as multiplicative terms (such as equation 7 in Rigney et al. (2018) and the *Daily WTD-T_{air}*
768 model developed in this study) demonstrate a more balanced distribution of explanatory power
769 between each independent variable (Table S7). Nevertheless, equation [7] in Rigney et al. (2018)
770 remains predominantly influenced by the T_{air} component (Table S7). A more balanced distribution of
771 explanatory power between temperature and WTD is desirable, given that both variables are
772 recognized as key drivers of soil CO_2 flux dynamics, which is achieved better with the *Daily WTD-T_{air}*
773 than with any of the empirical models in Table S7.

774 We acknowledge that the *Daily WTD-T_{air} model* does not reproduce many of the highest observed fCO_2
775 values (Figure S6 and S7). In addition to identifying a relationship between fCO_2 and WTD, which was
776 used to derive the *Daily WTD-T_{air} model* (Figure S5), we studied the temperature sensitivity within
777 WTD bins to better understand the model's inability to reproduce the highest observed fCO_2 values.
778 Specifically, we binned the daily fCO_2 into four WTD intervals: <20 cm (n=73), 20 to 40 cm (n=37), 30 to
779 40 cm (n=77) and >40 cm (n=44) (Figure S9). We identified a potential relationship between fCO_2 and
780 temperature within WTD bins (Figure S9). This result is expected given the strong interdependence
781 among fCO_2, temperature and WTD, all of which exhibit comparable seasonal dynamics. The high
782 observed fCO_2 values cannot be captured by a simple empirical model based solely on T_{air} and WTD,
783 particularly because both high and low fCO_2 occur under similar T_{air} and WTD conditions (Figure S5, S7
784 and S9). Consequently, the *Daily WTD-T_{air} model* represents a compromise that captures part of the
785 variability while preserving a realistic mean response.

786 In this study, we demonstrate the need for the development of emission models operating on a sub-
787 annual timescale. It highlights the necessity of creating scalable generalized models based on
788 temperature, WTD and possibly other predictors. The development of such models requires data from
789 a large number of sites with continuous and temporally dense measurement, in order to integrate
790 information in a manner similar to models based on annual WTD. We recognize that currently, models
791 based on annual WTD are likely the most robust for upscaling to national level and current conditions.

792 The simulated soil CO_2 flux at Vejrumbro, estimated using the *Daily WTD-T_{air}* model (13.6 Mg CO_2-C ha$^-$
793 ^{1} yr^{-1}), aligns well with flux measurements from Danish and German sites (Figure 5). This agreement
794 suggests a comparable magnitude of emissions across geographically distinct locations of similar
795 characteristics, such as soil type and land use history.

796 We acknowledge that the *Daily WTD-T_{air} model* is derived from a single dataset, and that other
797 emission models also provide valid fits of WTD and T_{air}. Furthermore, we recognize that empirical
798 emission models are highly dependent on the specific data to which they are fitted. Acknowledging the
799 limited data behind the *Daily WTD-T_{air} model* utilized in this study, the goal has not been to accurately
800 estimate the peatland emission budget, which will be uncertain due to the reliance on a single site.
801 However, the objective has been to illustrate the impact and insights gained from applying emission
802 models at a daily timescale and how this has significant impact on the conclusions that can be made
803 regarding effects of rewetting and climate change. The decision to utilize the *Daily WTD-T_{air} model* for
804 rewetting and climate modeling scenarios is motivated by the simplicity of the relationship and its
805 direct derivation from the Vejrumbro data, which clearly demonstrates a temperature-dependent
806 relationship between soil CO_2 flux and WTD. The limited availability of multiple high-temporal-
807 resolution GHG emission datasets broadly restricts the ability to generalize and upscale empirical GHG
808 emission models at a daily timescale. Therefore, we consider the *Daily WTD-T_{air}* model to be the most
809 reliable option currently available. Future research should validate the performance of emission
810 models on intra-annual (within years) data with continuous measured CO_2 data.

811 A promising methodology for future applications, as well as for integrating a Tier 3 framework,
812 involves coupling a process-based hydrological model with process-based emission models or an
813 empirically derived daily emission model, such as the one developed in this study, to enable detailed
814 simulations of GHG emissions that capture short-term dynamics and compound environmental effects.

815

816

Conclusion

This study demonstrates the feasibility of simulating the temporal dynamics of the peatland water balance and shallow groundwater table depth (WTD) using a catchment-scale distributed hydrological model. Accurately modelling shallow WTD is critical for reliable projections of CO_2 emissions from peatlands. We combined simulations of shallow WTD from the calibrated hydrological model with two empirical CO_2 emission models 1) an annual WTD-CO_2 relationship and 2) a daily WTD-CO_2 model accounting for the temperature effect on soil CO_2 production. This approach was used to estimate net soil CO_2 emissions for the historical period (1991-2020), the mid-century period (2041-2070) and the end-of-century period (2071-2100). This demonstrated that projections of soil CO_2 emissions are highly sensitive to the complexity and temporal resolution of the emission model applied. Specifically, models that incorporate both temperature and WTD dynamics at a daily timescale results in vastly different conclusion regarding impacts of climate change and rewetting. Regarding climate change impacts, we show that a daily temperature and WTD based emission model predict increased emissions due to temperature changes, which can be counter balanced (in the Danish case) or amplified depending on the future trend in WTD. Our results also demonstrate that rewetting strategies aimed at raising the groundwater table during the warm summer period offer a CO_2 emission reduction potential of up to 50%, whereas approaches focused primarily on increasing winter water table levels result in only marginal reductions. The combination of process-based hydrological model simulations and a daily-resolution empirical CO_2 emission model used in this study captures the influence of short-term compound climate events—such as simultaneous high temperatures and low WTD—which substantially alters projected emission trends compared to simpler approaches. Such refined approaches are essential for developing adaptive, climate-resilient peatland restoration policies and improving national greenhouse gas inventories. The findings underscore the importance of moving beyond static, annual WTD thresholds in peatland management by incorporating dynamic hydrological simulations. Instead, rewetting strategies should prioritize maintaining elevated summer groundwater table levels to buffer against drought-induced emission peaks.

Supplement link

…

Author contributions

All authors contributed to the conception and design of the study. TD conducted the analysis and drafted the manuscript, with input and revisions from all co-authors.

Competing interests

The authors declare that they have no conflict of interest.

Acknowledgements

We would like to thank Independent Research Fund Denmark for supporting the project PEAtlands and Climate-driven variability in groundwater depth – Impacts on greenhouse gas Emissions.

References

Adhikari, K., Hartemink, A. E., Minasny, B., Bou Kheir, R., Greve, M. B., and Greve, M. H.: Digital mapping of soil organic carbon contents and stocks in Denmark, PLoS One, 9, https://doi.org/10.1371/journal.pone.0105519, 2014.

Ala-aho, P., Soulsby, C., Wang, H., and Tetzlaff, D.: Integrated surface-subsurface model to investigate

858   the role of groundwater in headwater catchment runoff generation: A minimalist approach to
859   parameterisation, J. Hydrol., 547, 664–677, https://doi.org/10.1016/j.jhydrol.2017.02.023, 2017.

860   Arents, E. J. M. M., van der Kolk, J. W. H., Hengeveld, G. M., Lesschen, J. P., Kramer, H., Kuikman, P. J.,
861   and Schelhaas, M. J.: Greenhouse gas reporting for the LULUCF sector in the Netherlands -
862   Methodological background, updata 2018, Wageningen, WOt-technical report 113., 2018.

863   Asadzadeh, M. and Tolson, B.: Pareto archived dynamically dimensioned search with hypervolume-
864   based selection for multi-objective optimization, Eng. Optim, 45, 1489–1509,
865   https://doi.org/https://doi.org/10.1080/0305215X.2012.748046, 2013.

866   Autio, A., Aho, P. A., Ronkanen, A. K., Rossi, P. M., and Kløve, B.: Implications of Peat Soil
867   Conceptualization for Groundwater Exfiltration in Numerical Modeling: A Study on a Hypothetical
868   Peatland Hillslope, Water Resour. Res., https://doi.org/10.1029/2019WR026203, 2020.

869   Bechtold, M., Tiemeyer, B., Laggner, A., Leppelt, T., Frahm, E., and Belting, S.: Large-scale
870   regionalization of water table depth in peatlands optimized for greenhouse gas emission upscaling,
871   Hydrol. Earth Syst. Sci., 18, 3319–3339, https://doi.org/10.5194/hess-18-3319-2014, 2014.

872   Bechtold, M., Lannoy, G. J. M. De, Koster, R. D., Reichle, R. H., Mahanama, S. P., Bleuten, W.,
873   Bourgault, M. A., Brümmer, C., Burdun, I., Desai, A. R., Devito, K., Grünwald, T., Grygoruk, M.,
874   Humphreys, E. R., Klatt, J., Kurbatova, J., Lohila, A., Munir, T. M., Nilsson, M. B., Price, J. S., Röhl, M.,
875   Schneider, A., and Tiemeyer, B.: PEAT-CLSM: A Specific Treatment of Peatland Hydrology in the NASA
876   Catchment Land Surface Model, J. Adv. Model. Earth Syst., 2130–2162,
877   https://doi.org/10.1029/2018MS001574, 2019.

878   Bechtold, M., Lannoy, G. J. M. De, Reichle, R. H., Roose, D., Balliston, N., Burdun, I., Devito, K.,
879   Kurbatova, J., Strack, M., Zarov, E. A., States, U., Hydrology, W., Sciences, B., and Climate, G.: Improved
880   Groundwater Table and L-band Brightness Temperature Estimates for Northern Hemisphere Peatlands
881   Using New Model Physics and SMOS Observations in a Global Data Assimilation Framework, Remote
882   Sens. Environ., 246, 2020.

883   Bleuten, W., Zarov, E., and Schmitz, O.: A high-resolution transient 3-dimensional hydrological model
884   of an extensive undisturbed bog complex in West Siberia, Mires Peat, 26, 1–25,
885   https://doi.org/10.19189/MaP.2019.OMB.StA.1769, 2020.

886   Bona, K. A., Shaw, C., Thompson, D. K., Hararuk, O., Webster, K., Zhang, G., Voicu, M., and Kurz, W. A.:
887   The Canadian model for peatlands (CaMP): A peatland carbon model for national greenhouse gas
888   reporting, Ecol. Modell., 431, 109164, https://doi.org/10.1016/j.ecolmodel.2020.109164, 2020.

889   Børgesen, C. D., Waagepetersen, J., Iversen, T. M., Grant, R., Jacobsen, B., and Elmhold, S.:
890   Midtvejsevaluering af vandmiljøplan III - Hoved- og baggrundsnotater, 2009.

891   Bradley, C.: Simulation of the annual water table dynamics of a foodplain wetland, Narborough Bog ,
892   UK, J. Hydrol., 261, 150–172, 2002.

893   DHI: MIKE HYDRO - River - User Guide, Hørsholm, Denmark, 2019.

894   DHI: MIKE SHE - User Guide and Reference Manual, Hørsholm, Denmark, 2022.

895   Duranel, A., Thompson, J. R., Burningham, H., Durepaire, P., Garambois, S., Wyns, R., and Cubizolle, H.:
896   Modelling the hydrological interactions between a fissured granite aquifer and a valley mire in the
897   Massif Central, France, Hydrol. Earth Syst. Sci., 25, 291–319, 2021.

898   Evans, C. D., Peacock, M., Baird, A. J., Artz, R. R. E., Burden, A., Callaghan, N., Chapman, P. J., Cooper,
899   H. M., Coyle, M., Craig, E., Cumming, A., Dixon, S., Gauci, V., Grayson, R. P., Helfter, C., Heppell, C. M.,
900   Holden, J., Jones, D. L., Kaduk, J., Levy, P., Matthews, R., McNamara, N. P., Misselbrook, T., Oakley, S.,
901   Page, S. E., Rayment, M., Ridley, L. M., Stanley, K. M., Williamson, J. L., Worrall, F., and Morrison, R.:

902   Overriding water table control on managed peatland greenhouse gas emissions, Nature, 593, 548–552,
903   https://doi.org/10.1038/s41586-021-03523-1, 2021.

904   Friedrich, S., Gerner, A., Gabrielle, C., and Disse, M.: Scenario-based groundwater modeling of a raised
905   bog with Mike She, EGU Gen. Assem. 2023, Vienna, Austria, 24–28 Apr 2023, EGU23-15608,
906   https://doi.org/https://doi.org/10.5194/egusphere-egu23-15608, 2023.

907   Jupiter: https://www.geus.dk/produkter-ydelser-og-faciliteter/data-og-kort/national-boringsdatabase-
908   jupiter, last access: 12 April 2025.

909   Graham, D. N. and Butts, M. B.: Flexible Integrated Watershed Modeling with MIKE SHE, in: Watershed
910   Models, edited by: Singh, V. P. and Frevert, D. K., CRC Press, 245–272,
911   https://doi.org/10.1201/9781420037432.ch10, 2005.

912   Günther, A., Barthelmes, A., Huth, V., Joosten, H., Jurasinski, G., Koebsch, F., and Couwenberg, J.:
913   Prompt rewetting of drained peatlands reduces climate warming despite methane emissions, Nat.
914   Commun., 11, 1–5, https://doi.org/10.1038/s41467-020-15499-z, 2020.

915   Gyldenkærne, S., Callisen, L. W., Greve, M. H., Beucher, A. M., Weber, P. L., Elsgaard, L., Lærke, P. E.,
916   Stisen, S., Koch, J., and Levin, G.: Opgørelse af CO2-emissioner fra organiske jorde, Aarhus Universitet,
917   DCE – Nationalt Center for Miljø og Energi, Fagligt notat nr. 2025|01, 29pp pp., 2025.

918   Haahti, K., Warsta, L., Kokkoneen, T., Younis, B. B., and Koivusalo, H.: Distributed hydrological modeling
919   with channel network flow of a forestry drained peatland site, Water Resour. Res., 246–263,
920   https://doi.org/10.1002/2015WR018038.Received, 2015.

921   Henriksen, H. J., Kragh, S. J., Gotfredsen, J., Ondracek, M., M, van, T., Jakobsen, A., Schneider, R., Koch,
922   J., Troldborg, L., Rasmussen, P., Pasten-Zapata, E., and Stisen, S.: Dokumentationsrapport vedr.
923   modelleverancer til Hydrologisk Informations- og Prognosesystem, 2020.

924   Henriksen, H. J., Schneider, R., Koch, J., Ondracek, M., Troldborg, L., Seidenfaden, I. K., Kragh, S. J.,
925   Bøgh, E., and Stisen, S.: A New Digital Twin for Climate Change Adaptation, Water Management, and
926   Disaster Risk Reduction (HIP Digital Twin), Water (Switzerland), 15,
927   https://doi.org/10.3390/w15010025, 2023.

928   IPCC: 2013 Supplement to the 2006 IPCC Guidelines for National Greenhouse Gas Inventories :
929   Wetlands, edited by: Hiraishi, T., Krug, T., Tanabe, K., Srivastava, N., Baasansuren, J., Fukuda,
930   M.Troxler, T. G., Published: IPCC, Switzerland, Switzerland, 2014.

931   Jacob, D., Petersen, J., Eggert, B., Alias, A., Christensen, O. B., Bouwer, L. M., Braun, A., Colette, A.,
932   Déqué, M., Georgievski, G., Georgopoulou, E., Gobiet, A., Menut, L., Nikulin, G., Haensler, A.,
933   Hempelmann, N., Jones, C., Keuler, K., Kovats, S., Kröner, N., Kotlarski, S., Kriegsmann, A., Martin, E.,
934   van Meijgaard, E., Moseley, C., Pfeifer, S., Preuschmann, S., Radermacher, C., Radtke, K., Rechid, D.,
935   Rounsevell, M., Samuelsson, P., Somot, S., Soussana, J. F., Teichmann, C., Valentini, R., Vautard, R.,
936   Weber, B., and Yiou, P.: EURO-CORDEX: New high-resolution climate change projections for European
937   impact research, Reg. Environ. Chang., 14, 563–578, https://doi.org/10.1007/s10113-013-0499-2,
938   2014.

939   Jaros, A., Rossi, P. M., Ronkanen, A., and Kløve, B.: Parameterisation of an integrated groundwater-
940   surface water model for hydrological analysis of boreal aapa mire wetlands, J. Hydrol., 575, 175–191,
941   https://doi.org/10.1016/j.jhydrol.2019.04.094, 2019.

942   Java, O., Kohv, M., and Lõhmus, A.: Performance of a bog hydrological system dynamics simulation
943   model in an ecological restoration context: Soomaa case study, Estonia, Water (Switzerland), 13,
944   https://doi.org/10.3390/w13162217, 2021.

945   Jutebring, E., Johansson, E., Sjöberg, Y., Huseby, R., and Laudon, H.: Groundwater-surface water

interactions across scales in a boreal landscape investigated using a numerical modelling approach, J. Hydrol., 560, 184–201, https://doi.org/10.1016/j.jhydrol.2018.03.011, 2018.

Kirpotin, S. N., Antoshkina, O. A., Berezin, A. E., Elshehawi, S., Feurdean, A., Lapshina, E. D., Pokrovsky, O. S., Peregon, A. M., Semenova, N. M., Tanneberger, F., Volkov, I. V, and Volkova, I. I.: Great Vasyugan Mire: How the world's largest peatland helps addressing the world's largest problems, Ambio, 50, 2038–2049, https://doi.org/10.1007/s13280-021-01520-2, 2021.

Koch, J., Elsgaard, L., Greve, M. H., Gyldenkærne, S., Hermansen, C., Levin, G., Wu, S., and Stisen, S.: Water-table-driven greenhouse gas emission estimates guide peatland restoration at national scale, Biogeosciences, 20, 2387–2403, https://doi.org/https://doi.org/10.5194/bg-20-2387-2023, 2023.

Lambert, C., Larocque, M., Gagné, S., and Garneau, M.: Aquifer-Peatland Hydrological Connectivity and Controlling Factors in Boreal Peatlands, Front. Earts Sci., 10, https://doi.org/10.3389/feart.2022.835817, 2022.

Largeron, C., Krinner, G., Ciais, P., and Brutel-Vuilmet, C.: Implementing northern peatlands in a global land surface model: Description and evaluation in the ORCHIDEE high-latitude version model (ORC-HL-PEAT), Geosci. Model Dev., 11, 3279–3297, https://doi.org/10.5194/gmd-11-3279-2018, 2018.

Leifeld, J., Wüst-Galley, C., and Page, S.: Intact and managed peatland soils as a source and sink of GHGs from 1850 to 2100, Nat. Clim. Chang., 9, 945–947, https://doi.org/10.1038/s41558-019-0615-5, 2019.

Lewis, C., Albertson, J., Zi, T., Xu, X., and Kiely, G.: How does afforestation affect the hydrology of a blanket peatland? A modelling study, Hydrol. Process., 3588, 3577–3588, https://doi.org/10.1002/hyp.9486, 2013.

Lloyd J., Taylor, J. A.: On the Temperature Dependence of Soil Respiration, Funct. Ecol., 8, 315–323, 1994.

Matott, L. S.: OSTRICH – An Optimization Software Toolkit for Research Involving Computational Heuristics Documentation and User's Guide, Version 17.12.19, New York, 2019.

Mozafari, B., Bruen, M., Donohue, S., Renou-wilson, F., and Loughlin, F. O.: Peatland dynamics: A review of process-based models and approaches Science of the Total Environment Peatland dynamics : A review of process-based models and approaches, Sci. Total Environ., 877, https://doi.org/10.1016/j.scitotenv.2023.162890, 2023.

Naturstyrelsen: Lavbundsprojekt Ringfenner, Detail- og Myndighedsprojekt, 2022.

Nielsen, A. S., Larsen, K. S., Lærke, P. L., Rodriguez, A. F., Pullens, J. W. M., Petersen, R. J., and Christiansen, J. R.: A full year of continuous net soil and ditch CO2, CH4, N2O fluxes, soil hydrology and meteorology for a drained fen in Denmark, Earth Syst. Sci. Data Discuss. [preprint], https://doi.org/10.5194/essd-2025-123, 2025a.

Nielsen, O.-K., Plejdrup, M. S., Winther, M., Nielsen, M., Gyldenkærne, S., Mikkelsen, M. H., Albrektsen, R., Hjelgaard, K., Fauser, P., Bruun, H. G., Levin, G., Callisen, L. W., Andersen, T. A., Johannsen, V. K., Nord-Larsen, T., Vesterdal, L., Stupak, I., Scott-Bentsen, N., Rasmussen, E., Petersen, S. B., Baunbæk, L., and Hansen, M. G.: Denmark's National Inventory Document 2025. Emission Inventories 1990-2023 - Submitted under the United Nations Framework Convention on Climate Change and the Paris Agreement, 2025b.

Oikawa, P. Y., Jenerette, G. D., Knox, S. H., Sturtevant, C., Verfaillie, J., Dronova, I., Poindexter, C. M., Eichelmann, E., and Baldocchi, D. D.: Evaluation of a hierarchy of models reveals importance of substrate limitation for predicting carbon dioxide and methane exchange in restored wetlands, J. Geophys. Res. Biogeosciences, 122, 145–167, https://doi.org/10.1002/2016JG003438, 2017.

Olefeldt, D., Euskirchen, E. S., Harden, J., Kane, E., McGuire, A. D., Waldrop, mark P., and Turetsky, M. R.: A decade of boreal rich fen greenhouse gas fluxes in response to natural and experimental water table variability, Glob. Chang. Biol., 23, 2428–2440, https://doi.org/10.1111/gcb.13612, 2017.

Pasten-Zapata, E., Sonnenborg, T. O., and Refsgaard, J. C.: Climate change: Sources of uncertainty in precipitation and temperature projections for Denmark, Geol. Surv. Denmark Greenl. Bull., 43, 1–6, https://doi.org/10.34194/GEUSB-201943-01-02, 2019.

Regeringen: Aftale om et Grønt Danmark - Aftale mellem regeringen, Landbrug & Fødevarer, Danmarks Naturfredningsforening, Fødevareforbundet NNF, Dansk Metal, Dansk Industri og Kommunernes Landsforening - 24. juni 2024, 2024.

Regulation (EU) 2024/1991: of the European Parliament and of the Council of 24 June 2024 on nature restoration and amending Regulation (EU) 2022/869, Official Journal of the European Union, 2024.

Rigney, C., Wilson, D., Renou-Wilson, F., Müller, C., Moser, G., and Byrne, K. A.: Greenhouse gas emissions from two rewetted peatlands previously managed for forestry, Mires Peat, 21, 1–23, https://doi.org/10.19189/MaP.2017.OMB.314, 2018.

Rodriguez, A. F., Pullens, J. W. M., Christiansen, J. R., Larsen, K. S., and Lærke, P. E.: Modeling of greenhouse gas emissions from paludiculture in rewetting peatlands is improved by high frequency water table data, Egusph. [preprint], https://doi.org/10.5194/egusphere-2024-3030, 2024.

Rossi, P. M., Ala-aho, P., and Doherty, J.: Impact of peatland drainage and restoration on esker groundwater resources: modeling future scenarios for management, Hydrogeol. J., 1131–1145, https://doi.org/10.1007/s10040-014-1127-z, 2014.

Scharling, M.: Klimagrid Danmark - Nedbør, lufttemperatur og potentiel fordampning 20X20 & 40x40 km - Metodebeskrivelse, Danish Meteorological Institute, 1999a.

Scharling, M.: Klimagrid Danmark Nedbør 10x10 km (ver. 2) - Metodebeskrivelse, Danish Meteorological Institute, 1999b.

Schneider, R., Koch, J., Troldborg, L., Henriksen, H. J., and Stisen, S.: Machine learning-based downscaling of modelled climate change impacts on groundwater table depth, 2022.

Seidenfaden, I. K., Sonnenborg, T. O., Stisen, S., and Kidmose, J.: Quantification of climate change sensitivity of shallow and deep groundwater in Denmark, J. Hydrol. Reg. Stud., 41, 101100, https://doi.org/10.1016/j.ejrh.2022.101100, 2022.

Shi, X., Thornton, P. E., Ricciuto, D. M., Hanson, P. J., Mao, J., Sebestyen, S. D., Griffiths, N. A., and Bisht, G.: Representing northern peatland microtopography and hydrology within the Community Land Model, Biogeosciences, 12, 6463–6477, https://doi.org/10.5194/bg-12-6463-2015, 2015.

Stenberg, L., Haahti, K., Hökkä, H., Launiainen, S., and Nieminen, M.: Hydrology of Drained Peatland Forest: Numerical Experiment on the Role of Tree Stand Heterogeneity and Management, For. MDPI, 1–19, https://doi.org/10.3390/f9100645, 2018.

Stisen, S., Sonnenborg, T. O., Troldborg, L., and Refsgaard, J. C.: Evaluation of Climate Input Biases and Water Balance Issues Using a Coupled Surface – Subsurface Model, Vadose Zo. J., 10, https://doi.org/10.2136/vzj2010.0001, 2011.

Stisen, S., Ondracek, M., Troldborg, L., Schneider, R. J. M., and van Til, M. J.: National Vandressource Model - Modelopstilling og kalibrering af DK-model 2019, De nationale geologiske undersøgelser for Danmark og Grønland (GEUS), Rapport 2019/31, 2019.

Tanneberger, F., Abel, S., Couwenberg, J., Dahms, T., Gaudig, G., Günther, A., Kreyling, J., Peters, J., Pongratz, J., and Joosten, H.: Towards net zero CO2 in 2050: An emission reduction pathway for

1033 organic soils in germany, Mires Peat, 27, 1–17, https://doi.org/10.19189/MaP.2020.SNPG.StA.1951,
1034 2021.

1035 Thompson, C., Devito, K. J., and Mendoza, C. A.: Hydrologic impact of aspen harvesting within the
1036 subhumid Boreal Plains of Alberta, Hydrol. Process., 3924–3937, https://doi.org/10.1002/hyp.13301,
1037 2018.

1038 Tiemeyer, B., Freibauer, A., Borraz, E. A., Augustin, J., Bechtold, M., Beetz, S., Beyer, C., Ebli, M.,
1039 Eickenscheidt, T., Fiedler, S., Förster, C., Gensior, A., Giebels, M., Glatzel, S., Heinichen, J., Hoffmann,
1040 M., Höper, H., Jurasinski, G., Laggner, A., Leiber-Sauheitl, K., Peichl-Brak, M., and Drösler, M.: A new
1041 methodology for organic soils in national greenhouse gas inventories: Data synthesis, derivation and
1042 application, Ecol. Indic., 109, 105838, https://doi.org/10.1016/j.ecolind.2019.105838, 2020.

1043 Wilson, D., Blain, D., Couwenber, J., Evans, C., Murdiyarso, D., Page, S., Renou-Wilson, F., Rieley, J.,
1044 Strack, M., and Tuittila, E. S.: Greenhouse gas emission factors associated with rewetting of organic
1045 soils, Mires Peat, 17, 1–28, https://doi.org/10.19189/MaP.2016.OMB.222, 2016.

1046 Wu, Y. and Blodau, C.: PEATBOG: A biogeochemical model for analyzing coupled carbon and nitrogen
1047 dynamics in northern peatlands, Geosci. Model Dev., 6, 1173–1207, https://doi.org/10.5194/gmd-6-
1048 1173-2013, 2013.

1049 Wunsch, A., Liesch, T., and Broda, S.: Deep learning shows declining groundwater levels in Germany
1050 until 2100 due to climate change, Nat. Commun., 13, 1–13, https://doi.org/10.1038/s41467-022-
1051 28770-2, 2022.

1052 Yuan, F., Wang, Y., Ricciuto, D. M., Shi, X., Yuan, F., Brehme, T., Bridgham, S., Keller, J., Warren, J. M.,
1053 Griffiths, N. A., Sebestyen, S. D., Hanson, P. J., Thornton, P. E., and Xu, X.: Hydrological feedbacks on
1054 peatland CH4 emission under warming and elevated CO2: A modeling study, J. Hydrol., 603, 127137,
1055 https://doi.org/10.1016/j.jhydrol.2021.127137, 2021.

1056 Zscheischler, J., Martius, O., Westra, S., Bevacqua, E., Raymond, C., Horton, R. M., van den Hurk, B.,
1057 AghaKouchak, A., Jézéquel, A., Mahecha, M. D., Maraun, D., Ramos, A. M., Ridder, N. N., Thiery, W.,
1058 and Vignotto, E.: A typology of compound weather and climate events, Nat. Rev. Earth Environ., 1,
1059 333–347, https://doi.org/10.1038/s43017-020-0060-z, 2020.

1060

1061